Progress of Theoretical Physics, Vol. 88, No. 5, November 1992

Perturbations of the Cosmic Microwave Background Radiation and Structure Formations

Naoshi SUGIYAMA and Naoteru GOUDA*

Department of Physics, The University of Tokyo, Tokyo 113
**Department of Earth and Space Science, Faculty of Science*
Osaka University, Toyonaka 560

(Received September 17, 1992)

After the recent discovery of temperature fluctuations of the cosmic microwave background radiation by *COBE*, the study of the temperature fluctuations becomes more and more important for understanding formations of large scale structures of the universe. The treatments for the evolution of small density fluctuations of matters and radiation by gauge invariant formalism are summarized. And the expected values of temperature anisotropies in various cosmological models are shown. Both flat and open universe models with and without the cosmological constant are considered. As for open universe models, in particular, any work had never been done by the complete treatment on large scale anisotropies. However we could find the complete formula to handle large scale temperature anisotropies and here this formula is adopted. Using the results of *COBE* with previous measurements of temperature fluctuations which give the upper limits, severe and reliable constraints on various cosmological models are obtained. As a result, it is found that the desirable models are the dark matter dominated universe models with initially scale free power spectrum and the density parameter $\Omega_0 \simeq 1$ while some models with low density are still allowed if the models have totally flat geometry by including the cosmological constant.

§ 1. Introduction

Since the discovery of Cosmic Microwave Background Radiation (CMB) by Penzias and Wilkinson at 1964,[1] CMB has been one of the most important objects of study for cosmologists. It directly shows us the feature of the universe at the last scattering time of photon with baryon. This time is the earliest epoch of the universe we can show by light. The energy spectrum of CMB takes completely black body form, as was shown by the Cosmic Microwave Background Explore (*COBE*).[2] This means that thermal equilibrium state was realized in the universe at the last scattering epoch and anything producing such large thermal energy that distorts the CMB has never happened after this epoch. This fact strongly supports the standard Big Bang model of the universe. The black body temperature is 2.735 ± 0.06 K and it is almost independent of the direction. This isotropy of the black body temperature is regarded as the direct evidence of the isotropy and homogeneity of the universe on large scales.

On the other hand, we know our universe has the variety of structures such as stars, globular clusters, galaxies, clusters of galaxies and so forth. And as the proceeding of the observations, more giant structures are appearing. These structures are understood as the objects originated from the small fluctuations in the isotropic and homogeneous background at the early epoch of the universe. Before the baryon-photon decoupling time, baryon and photon are strongly interacted by the Thomson scattering. Then if the density distributions of baryon fluctuate, the

density fluctuations of photon are also given rise to and the behavior of time evolution of both fluctuations are approximately the same. As the recombination process of hydrogen atom progresses, their interaction becomes weak. After all, baryon fluctuations have been freely growing up since the last scattering epoch without the pressure. These fluctuations are considered becoming present large scale structures. Hence we can expect to find seeds of fluctuations in the CMB. Until the recent discovery of *COBE* group,[3] however, no temperature fluctuations had been found except the dipole moment of anisotropies which is produced by our peculiar motion relative to the CMB rest frame. The observational limits of the temperature fluctuations $\delta T/T$ became lower and lower, and it reached almost 10^{-5}. This extreme isotropy of CMB gave the most severe and reliable constraints on the various cosmological models. Desirable models must produce enough density fluctuations of matter to make large scale structures of the universe without producing too much value of temperature fluctuations.

For example, it is known that the simple baryon dominated universe model was difficult to survive. This is one of the reasons to consider nonbaryonic dark matter. Dark matter was originally motivated by explaining the discrepancy between the luminous mass of the universe and the mass estimated by dynamical methods. The nonbaryonic dark matter is classified as hot (HDM), warm (WDM) and cold (CDM) according to how large the kinetic energies of the constituent particles of the dark matter are. Among them, CDM has been considered the most desirable one bacause CDM scenario has an advantage for explaining the fomation of the hierarchical structure in the universe. Such dark matter decouple with photon at very early time in the universe. And their density fluctuations were growing up faster than those of baryon because nonbaryonic dark matter are not affected by the photon pressure. Hence density fluctuations of matter may become enough larger than those of photon to explain the existence of large scale structures with small anisotropies of the CMB. However, the observational upper bound of the CMB anisotropies rapidly lowered since late '80s and it became more and more difficult to find a consistent model with observations. Moreover, the recent progress of the deep survey of the universe shows us new and larger structures such as Great Wall,[4] Great Attractor[5] and so on. It is diffiucult for CDM to make such large objects. Now, it looks like that the paradigm of the CDM scenario stands for the difficulty. Instead of the structure formation by CDM or other dark matter candidates, recently, the structure formation by topological defect such as string, domain wall and texture began to be considered. These defects directly make nonlinear objects without the help of the self-gravitational field of these objects. Hence there had been the expectation to make structures without producing too much temperature fluctuations. However, it is not the case. The gravitational potential field of defects themselves or the resultant objects must reproduce temperature fluctuations. This is known as the Sacks-Wolfe effect.[6] These scenarios would also become difficult to survive if the observational upper bounds of CMB isotropy had decreased any more.

It was just the time when the cosmology faced on the confusion that *COBE* found the temperature fluctuations.[3] This detection is one of the most important observational results after the discovery of CMB itself. At last we can see the seeds of the

large scale structure of the universe on the last scattering surface. From the viewpoint of the structure formations, these observational data can be used to estimate the amplitude of the photon density fluctuations directly. Before this discovery, we usually estimated it theoretically from the amplitude of matter density fluctuations obtained by the observations of the large scale structures such as two point galaxy-galaxy correlation functions in cosmological models. Using this method, we could not escape the so-called biasing problem that is whether the light trace mass or not. Now we have obtained both density fluctuations and temperature fluctuations independently.

The linear analysis of the evolution of small fluctuations in spatially homogeneous, isotropic cosmological models was pioneered by Lifshifz.[7] This work was then extended by many workers. And many works[8)~10)] have been done for the analysis of density fluctuations and anisotropies of the CMB in photon-baryon system. Here we also briefly show the procedure of the linear analysis of density fluctuations. Then we compare the expected temperature anisotropies in models of the structure formations with the data by *COBE* and other upper limits on small angular scales and give constraints on the models and cosmological parameters. We consider almost all representative cosmological scenarios, that is, baryon, cold dark matter or hot dark matter dominated models with initially adiabatic and isocurvature perturbations. Peebles' fully reionized universe models[12] are also shown. As for models with the cosmological densiy parameter, $\Omega_0 < 1.0$, both open geometry and flat one with cosmological constant are treated. As for the evolution of fluctuations, we adopt the gauge-invariant formalism of Bardeen[13] which is further developed by Kodama and Sasaki.[14] This method has several obvious advantages over the conventional synchronous gauge method because there exists no unphysical mode in the perturbation variables and it is easy to set a correct initial condition accurately in numerical calculations especially for isocurvature perturbations. Treating large scale temperature anisotropies, in particular, we use complete formula even in the open geometry[15] and calculate the quadrupole moment for all universe models considered here. Since *COBE* found the quadrupole and large scale anisotropies, we believe this complete treatment increases its importance.

The plan of the paper is as follows: In § 2, we review the method for analyzing the evolution of fluctuations by the gauge-invariant formula. Various cosmological models of structure formations based on the gravitational instability are shown in § 3. The brief review of observations on CMB anisotropies including the recent discovery of *COBE* and the constraints on cosmological models from these observational results are given in § 4. Other effects on CMB anisotropies which produce fluctuations between last scattering surface and present are shown in § 5. Finally, § 6 is devoted to conclusions and discussion.

§ 2. Methods

2.1. *The unperturbed background*[16),17)]

We assume that the matter is distributed uniformly and isotropic in the very early

universe. Then the unperturbed background is assumed to be described by a Robertson-Walker metric,

$$ds^2=-dt^2+a^2\gamma_{ij}dx^i dx^j,$$

$$\gamma_{ij}=\frac{dr^2}{1-Kr^2}+r^2d\Omega^2. \tag{2·1}$$

Here $d\Omega^2$ is the metric of the 2-dimensional Euclidean sphere and K is an constant curvature. The energy momentum tensor takes a perfect fluid form

$$T_{\mu\nu}=(\rho+p)u_\mu u_\nu+pg_{\mu\nu}, \tag{2·2}$$

$$\rho=\sum_\alpha \rho_\alpha, \quad p=\sum_\alpha p_\alpha, \tag{2·3}$$

where ρ_α and p_α denote unperturbed energy density and pressure for α-component (e.g., for baryon; $\alpha=b$ and for photon; $\alpha=r$). And u_μ is the 4-velocity, $(u^\mu)=(a^{-1}, 0, 0, 0)$. The Einstein equations are reduced to the two equations

$$\left(\frac{\dot{a}}{a}\right)^2+\frac{K}{a^2}=\frac{8\pi G}{3}\rho+\frac{\Lambda}{3}, \tag{2·4}$$

$$\dot{\rho}=-3\frac{\dot{a}}{a}h, \tag{2·5}$$

where

$$h\equiv\rho+p. \tag{2·6}$$

Here Λ is a cosmological constant and $(\dot{})=d/dt$. In this paper, we adopt the unit $c=1$.

2.2. *Perturbation in gauge-invariant scheme*

As mentioned in § 1, it is desirable to adopt the gauge-invariant scheme in the cosmological perturbation analysis. Here at first the variables representing perturbations are introduced and next the gauge invariant perturbed variables are constructed.

1) Perturbed variables

We consider only scalar perturbations (i.e., density perturbations) which are the only type of perturbations that would grow after docoupling and are of interest with respect to the problem of structure formations. In general, a perturbed metric is represented by

$$\tilde{g}_{00}=-a^2[1+2A\mathrm{Y}],$$

$$\tilde{g}_{0j}=-a^2B\mathrm{Y}_j,$$

$$\tilde{g}_{ij}=a^2[\gamma_{ij}+2H_L\mathrm{Y}\gamma_{ij}+2H_T\mathrm{Y}_{ij}], \tag{2·7}$$

where a tilde denotes a perturbed quantity and Y is a scalar harmonics, that is, an eigenfunction of the spatial Laplace operator and Y_i and Y_{ij} are vectors and tensors associated with it. To be more specific, they are defined as follows:

$$\gamma^{ij}\mathrm{Y}_{|ij}=-k^2\mathrm{Y}\,,\quad \mathrm{Y}_i=-k^{-1}\mathrm{Y}_{|i}\,,\quad \mathrm{Y}_{ij}=k^{-2}\mathrm{Y}_{|ij}+\frac{1}{3}\gamma_{ij}\mathrm{Y}\,, \tag{2·8}$$

where $|$ is a covariant derivative with respect to γ_{ij} and an eigenvalue k is interpreted as a *wavenumber* (in what follows, the indices i and j run from 1 to 3, and μ and ν from 0 to 3). We omit the summation symbol with respect to the eigenvalues as well as the eigenvalue indices of harmonic functions because there is no coupling among the expansion coefficients of harmonic functions with different eigenvalues in the linear perturbation analysis.

Accordingly, the perturbed energy-momentum tensor $\tilde{T}^{\mu}_{(\alpha)\nu}$ has the following components:

$$\begin{aligned}
&\tilde{T}^{0}_{(\alpha)0}=-\rho_\alpha(1+\delta_\alpha\mathrm{Y})\,,\\
&\tilde{T}^{0}_{(\alpha)j}=(\rho_\alpha+p_\alpha)(v_\alpha-B)\mathrm{Y}_j\,,\\
&\tilde{T}^{j}_{(\alpha)0}=-(\rho_\alpha+p_\alpha)v_\alpha\mathrm{Y}^j\,,\\
&\tilde{T}^{i}_{(\alpha)j}=p_\alpha(\delta^i{}_j+\pi_{L\alpha}\mathrm{Y}\delta^i{}_j+\pi_{T\alpha}\mathrm{Y}_j{}^i)\,,
\end{aligned} \tag{2·9}$$

where ρ_α and p_α denote unperturbed energy-density and pressure for α-component. The quantities δ_α, v_α, $\pi_{L\alpha}$ and $\pi_{T\alpha}$ are perturbations with respect to energy density, spatial velocity and isotropic and anisotropic stresses. All of the above quantities can be regarded as functions only of time in the following perturbation equations.

2) Gauge-invariant variables[14]

In general relativistic perturbation theories, the notation of a perturbation variable loses its direct physical significance, especially on super-horizon scales, due to the presence of coordinate gauge freedom. Namely, the variables representing perturbations change under the change between the perturbed world and the unperturbed background. Then the amplitudes of perturbations in the metric and the energy-momentum tensor shown above are not invariant under this change of correspondence. The change of correspondence is called a gauge transformation and formally expressed in terms of a coordinate transformation in the perturbed world. A scalar type infinitesimal gauge transformation $(\eta, \boldsymbol{x})\to(\bar{\eta}, \bar{\boldsymbol{x}})$ is expressed as

$$\begin{aligned}
&\bar{\eta}=\eta+T\mathrm{Y}\,,\\
&\bar{x}^j=x^j+L\mathrm{Y}^j\,,
\end{aligned}$$

where η is a conformal time defined by $d\eta\equiv dt/a$ and T and L are arbitrary functions of time, being regarded as quantities of the same order as the perturbation variables. As stated in the Introduction, if we take the special gauge condition, such as synchronous gauge condition, which was used by many authors, we cannot completely eliminate gauge freedom and there leaves room for gauge modes to play an undesirable role in the perturbation analysis. On the other hand, we can discuss all kinds of cosmological perturbations without worrying about gauge modes if we adopt the gauge-invariant formalism, that is, we deal only with gauge-invariant perturbation variables which are defined to be invariant under gauge transformations. The gauge-invariant variables can be constructed by combining them in an appropriate

manner. As for metric perturbations there are two independent gauge-invariant quantities. A convenient choice of them is as follows:

$$\Phi \equiv H_L + \frac{1}{3}H_T + \frac{a'}{ak}\left(B - \frac{H_T'}{k}\right),$$

$$\Psi \equiv A + \frac{a'}{ak}\left(B - \frac{H_T'}{k}\right) + \frac{1}{k}\left(B' - \frac{H_T''}{k}\right) \tag{2·10}$$

with a prime denoting a derivative with respect to the conformal time η. The former, Φ, represents the perturbation to the intrinsic spatial curvature and, the latter Ψ, to the gravitational potential for Newtonian slicing, i.e., the gauge condition such that $k^{-1}H_T' - B = 0$.

Perturbations to the energy-momentum tensor yield four convenient gauge-invariant combinations; the density perturbation defined in the total matter center-of-mass frame $\Delta_{c\alpha}$, the shear of the four velocity V_α, the entropy perturbation Γ_α and the anisotropic stress perturbation Π_α. They are constructed out of ordinary (gauge-dependent) variables as follows:

$$\Delta_{c\alpha} \equiv \delta_\alpha + 3(1+w_\alpha)\frac{a'}{ak}(v - B),$$

$$V_\alpha \equiv v_\alpha - \frac{H_T'}{k},$$

$$\Gamma_\alpha \equiv \pi_{L\alpha} - \frac{c_\alpha{}^2}{w_\alpha}\delta_\alpha,$$

$$\Pi_\alpha \equiv \pi_{T\alpha}, \tag{2·11}$$

where v is the center-of-mass velocity of matter and

$$w_\alpha \equiv p_\alpha/\rho_\alpha,$$

$$c_\alpha{}^2 \equiv p_\alpha'/\rho_\alpha'. \tag{2·12}$$

Also for total matter, similar gauge-invariant variables are defined:

$$\Delta \equiv \rho^{-1}\sum_\alpha \rho_\alpha \Delta_{c\alpha},$$

$$V \equiv h^{-1}\sum_\alpha h_\alpha V_\alpha. \tag{2·13}$$

The non-adiabaticity of total matter Γ and anistropic stress perturbation Π are given by

$$\Gamma \equiv \Gamma_{\rm int} + \Gamma_{\rm rel},$$

$$\Pi = p^{-1}\sum_\alpha p_\alpha \Pi_\alpha, \tag{2·14}$$

where

$$\Gamma_{\rm int} \equiv p^{-1}\sum_\alpha p_\alpha \Gamma_\alpha,$$

$$\Gamma_{\rm rel}\equiv p^{-1}\sum_{\alpha}(c_\alpha{}^2-c_s{}^2)\rho_\alpha\Delta_{c\alpha}\,, \tag{2·15}$$

and $\Gamma_{\rm int}$ is the intrinsic entropy perturbation of each component, $\Gamma_{\rm rel}$ is that due to the difference of the dynamical behavior of each component and c_s is the sound velocity given by

$$c_s{}^2=\sum_{\alpha}c_\alpha{}^2\rho'_\alpha/\rho'\,. \tag{2·16}$$

From the perturbed Einstein equations, Φ and Ψ are expressed algebraically in terms of matter variables,

$$2(k^2-3K)\Phi=8\pi Ga^2\rho\Delta \tag{2·17}$$

and

$$\Phi+\Psi=-8\pi Ga^2pH/k^2\,. \tag{2·18}$$

This is one of the advantages of the gauge-invariant method. Since metric perturbations Φ and Ψ are expressed algebraically in terms of total matter variables, the equation for density perturbations becomes quadratic in the present gauge-invariant scheme, contrary to the quartic equation in a synchronous gauge.[14] This is the reason why there is no room for the mixing of unphysical gauge modes in the present scheme. As stated before, the fact that the unphysical gauge modes are not present in the gauge-invariant scheme results in the following merit: The use of synchronous gauge, which has often been used, is potentially dangerous and may lead to an incorrect result because it is very difficult to single out the purely growing mode numerically in the synchronous gauge and it allows to include a gauge mode in the synchronous gauge especially for isocurvature baryon dominated models. However we do not worry about the gauge mode in the gauge-invariant formalism.[11),18)~20)]

2.3. *Evolution equations of perturbations before decoupling*

The detailed evolution equations of perturbations are shown in §§ 2.3 and 2.4.[14),11),20)] Photon, baryon and other collisionless particles are considered as components of the universe and we analyze their density fluctuations.

To calculate the evolution of perturbations, we separate the history of the universe into three stages. The first stage is that the photon temperature is so high that the universe is fully ionized. The second stage is the era when the recombination process of hydrogen atom is working. After the universe being sufficiently optically thin, the final stage comes. In this subsection, the method of dealing with the evolution of perturbations in first two stages is explained. About the final stage, it is shown in § 2.5.

Here we intoduce a new gauge-invariant variable U_α which is defined as

$$U_\alpha\equiv V_\alpha-\frac{k}{Ha}\Phi\,, \tag{2·19}$$

in place of shear velocity V_α.

(1) $T_r\geq 6000\,\mathrm{K}$

This is the pre-recombination stage. Baryons and photons are coupled strongly and we can treat them together as viscous fluid. The perturbed density and pressure of this fluid component are expressed as $\rho_f=\rho_r+\rho_b$ and $p_f=p_r$. For each component, i.e., viscous fluid f and collisionless particles X the evolution equations of perturbations are expressed as

$$\frac{d\Delta_a}{da}=3\frac{w_a-{c_a}^2}{a}\Delta_{ca}-\frac{k}{Ha^2}(1+w_a)U_a-3\frac{w_a}{a}\Gamma_a-\frac{3}{2}\frac{1+K/(Ha)^2}{1-3K/k^2}\frac{1+w_a}{a}\Delta$$
$$+3\frac{1+w_a}{(1+w)a}\sum\frac{\rho_a}{\rho}\left[{c_a}^2\Delta_{ca}+w_a\Gamma_a-\frac{2}{3}w_a\left(1-\frac{3K}{k^2}\right)\Pi_a\right]$$
$$+\frac{3}{Ha^2}\frac{K}{k}(1+w_a)\left(U+\frac{3}{2}\frac{1+K/(Ha)^2}{1-3K/k^2}\frac{Ha}{k}\Delta\right), \tag{2·20}$$

$$\frac{dU_a}{da}=\frac{3{c_a}^2-1}{a}U_a+\frac{3}{2a}\left[(1+w)\left(1+\frac{K}{(Ha)^2}\right)-2c^2\right]U$$
$$+\frac{k}{Ha^2(1+w_a)}\left[{c_a}^2\Delta_{ca}+w_a\Gamma_a-\frac{2}{3}w_a\left(1-\frac{3K}{k^2}\right)\Pi_a\right]$$
$$+\frac{3}{2}\frac{K}{Ha^2k}\frac{1+K/(Ha)^2}{1-3K/k^2}\Delta, \tag{2·21}$$

where $w\equiv\sum p_a/\rho$ and $U\equiv\sum h_aU_a/\sum h_a$. For the viscous fluid component,

$$w_f\Gamma_f=-\frac{4\rho_r\rho_b}{9h_f\rho_f}S_{br} \tag{2·22}$$

and

$$w_f\Pi_f=\frac{16\rho_r}{27\rho_f}\frac{k\left(V_f-\frac{\rho_b}{h_f}V_{br}\right)}{HaR_c}, \tag{2·23}$$

where

$$R_c\equiv\frac{n_e\sigma_T}{H}=\frac{1}{Ht_c} \tag{2·24}$$

with n_e, σ_T and t_c being the electron number density, Thomson scattering cross section and the mean free time of electrons, respectively. Using the viscous fluid approximation, the relative velocity V_{br} between baryons and photons can be solved algebraically as

$$V_{br}\equiv V_b-V_r=U_b-U_r$$
$$=\frac{-\frac{\rho_f}{3h_f}\Delta_{cf}+\frac{\rho_b}{3h_f}S_{br}-\frac{Ha}{k}(U_f-U)+\frac{8}{27}\left(1-\frac{3K}{k^2}\right)\frac{k}{HaR_c}V_f}{\frac{Ha}{k}\left(\frac{h_f}{\rho_b}R_c+\frac{4\rho_r}{3h_f}\right)+\frac{8}{27}\left(1-\frac{3K}{k^2}\right)\frac{\rho_b}{h_f}\frac{k}{HaR_c}}. \tag{2·25}$$

The evolution equation of the entropy perturbation is as follows:

$$\frac{d}{da}S_{br}=-\frac{k}{Ha^2}V_{br}\,. \tag{2·26}$$

As for the collisionless particles X, Γ_X and Π_X are dependent on their characters. In case of cold dark matter, we do not have to consider these terms because kinematic energy of these particles can be neglected. On the other hand, hot dark matter has large kinematic energy in the early epoch. The collisionless Boltzmann equation must be solved to obtain Γ_X and Π_X.[21]

(2) $1000\,\mathrm{K}\leq T_r<6000\,\mathrm{K}$

On this stage, we treat baryons and photons separately since the recombination process plays a part. For each component except photons, the same equations as stage (1) are solved to calculate the time evolution. On the other hand, the collisional Boltzmann equation is solved for photon distribution function $\tilde{f}(x^\mu, q^\mu)$ as

$$q^\mu\frac{\partial\tilde{f}}{\partial x^\mu}+\frac{dq^\mu}{d\lambda}\frac{\partial\tilde{f}}{\partial q^\mu}=C[\tilde{f}]\,, \tag{2·27}$$

where λ is the affine parameter of photon trajectory and $C[\tilde{f}]$ is the collision term[22] given by

$$C[\tilde{f}]=\frac{3}{8\pi}n_e\sigma_T q\int d\bar{\Omega}_*\frac{1+\cos^2\bar{\theta}}{2}(\tilde{f}(x_*, q_*)-\tilde{f}(x, q))\,, \tag{2·28}$$

where $*$ refers to the quantities associated with a scattered photon and a bar to the values in the electron rest frame. Here we introduce the gauge invariant brightness function ϵ_{cr} as

$$\epsilon_{cr}(\eta, \boldsymbol{x}, \boldsymbol{\gamma})=\frac{4\pi}{\rho_r}\int\delta f q^3dq+\frac{4}{k}\left(\frac{a'}{a}(v-B)\mathrm{Y}+(v-B)\gamma^i\mathrm{Y}_{|i}\right), \tag{2·29}$$

where $\boldsymbol{\gamma}$ is the direction cosine of photon propagation. In order to calculate the Boltzmann equation, we expand ϵ_{cr} in accordance with Wilson[10] as

$$\epsilon_{cr}(\eta, \boldsymbol{x}, \boldsymbol{\gamma})=\sum_{l=0}^{\infty}\epsilon_{cr(l)}(\eta)(-k)^{-l}Y_{|i_1\cdots i_l}P_{(l)}^{i_1\cdots i_l}(\boldsymbol{x}, \boldsymbol{\gamma})\,. \tag{2·30}$$

$P_{(l)}^{i_1\cdots i_l}$ is an l-th rank tensor defined by

$$P_{(0)}\equiv 1\,,\quad P_{(1)}^i\equiv\gamma^i\,,$$

$$P_{(l+1)}^{i_1\cdots i_{l+1}}\equiv\frac{2l+1}{l+1}\gamma^{(i_1}P_{(l)}^{i_2\cdots i_{l+1})}-\frac{l}{l+1}\gamma^{(i_1i_2}P_{(l-1)}^{i_3\cdots i_{l+1})}\,. \tag{2·31}$$

Parentheses about indices indicate symmetrization of these indices. The previous photons perturbation variables are related to the first three terms of the expansion as

$$\Delta_{cr}=\epsilon_{cr(0)}\,,$$

$$V_r-V=U_r-U=\frac{1}{4}\epsilon_{cr(1)}\,,$$

$$\Pi_r=\frac{3}{5}\epsilon_{cr(2)}\,. \tag{2·32}$$

The evolution equations obtained from the Boltzmann equation are then

$$\frac{d}{da}\epsilon_{cr(0)}=-\frac{1}{3}\frac{k}{Ha^2}\epsilon_{cr(1)}-\frac{4}{3}\frac{k}{Ha^2}U-\frac{2}{a}\frac{1+K/(Ha)^2}{1-3K/k^2}\Delta$$
$$+\frac{4}{(1+w)a}\sum\frac{\rho_\alpha}{\rho}\left[c_\alpha{}^2\Delta_{c\alpha}+w_\alpha\Gamma_\alpha-\frac{2}{3}w_\alpha\left(1-\frac{3K}{k^2}\right)\Pi_\alpha\right]$$
$$+\frac{4}{Ha^2}\frac{K}{k}\left(U+\frac{3}{2}\frac{1+K/(Ha)^2}{1-3K/k^2}\frac{Ha}{k}\Delta\right), \tag{2·33}$$

$$\frac{d}{da}\epsilon_{cr(1)}=\frac{6}{a}\left[(1+w)\left(1+\frac{K}{(Ha)^2}\right)-\frac{2}{3}\right]U+6\frac{K}{Ha^2k}\frac{1+K/(Ha)^2}{1-3K/k^2}\Delta$$
$$+\frac{k}{Ha^2}\left[\epsilon_{cr(0)}-\frac{2}{5}\left(1-\frac{3K}{k^2}\right)\epsilon_{cr(2)}\right]-4\frac{d}{da}U-\frac{R_c}{a}(\epsilon_{cr(1)}+4U-4U_b), \tag{2·34}$$

$$\frac{d}{da}\epsilon_{cr(2)}=-\frac{9}{10}\frac{R_c}{a}\epsilon_{cr(2)}+\frac{k}{Ha^2}\left[\frac{2}{3}\epsilon_{cr(1)}+\frac{8}{3}V-\frac{3}{7}\left(1-\frac{8K}{k^2}\right)\epsilon_{cr(3)}\right],\quad l\geq 3, \tag{2·35}$$

$$\frac{d}{da}\epsilon_{cr(l)}=-\frac{R_c}{a}\epsilon_{cr(l)}+\frac{k}{Ha^2}\left[\frac{l}{2l-1}\epsilon_{cr(l-1)}-\frac{l+1}{2l+3}\left[1-\frac{l(l+2)}{k^2}K\right]\epsilon_{cr(l+1)}\right]. \tag{2·36}$$

In our calculations, we take the maximum number of l as 1000.

2.4. *Evolution equations of perturbations after decoupling*

The calculation based on the two fluid description is carried out until recombination of protons and electrons is effectively completed as shown in the previous subsection. We take this epoch to be at $T=1000$ K for the ordinary models except Peebles' model (see § 3). By this epoch, matter density perturbations are dominated by the growing mode. After that time, matter and photon perturbations begin to evolve independently. In the linear regime, the growing mode of matter density perturbations at present and at decoupling time ($z_{\rm dec}$) is related as:[16),17)]

$$\Delta_{cb}(z=0)=(1+z_{dec})\Delta_{cb}(z_{dec}) \tag{2·37}$$

for $\Omega_0=1$ (Ω_0 is the present value of the cosmological density parameter) and

$$\Delta_{cb}(z=0)=\frac{(\cosh\sqrt{-K}\,\eta_0-1)(\cosh\sqrt{-K}\,\eta_0+5)-3\sqrt{-K}\,\eta_0\sinh\sqrt{-K}\,\eta_0}{(\cosh\sqrt{-K}\,\eta_0-1)^3}$$
$$\times 5(1+z_{dec})\Delta_{cb}(z_{dec}) \tag{2·38}$$

for $\Omega_0<1$, where

$$\sqrt{-K}\,\eta_0\equiv\cosh^{-1}(2\Omega_0{}^{-1}-1). \tag{2·39}$$

The propagation of photon perturbations in an optically thin universe after $z=z_{\rm dec}$ is governed by the following equation:[15),19)]

$$\frac{d}{d\eta}[\Theta_s(\eta, \boldsymbol{x}(\eta), \boldsymbol{\gamma})+\Psi(\eta, \boldsymbol{x}(\eta))]$$

$$\equiv\frac{\partial}{\partial\eta}(\Theta_s+\Psi)+\gamma^i\frac{\partial}{\partial x^i}(\Theta_s+\Psi)-\Gamma^i_{jk}\gamma^j\gamma^k\frac{\partial}{\partial\gamma^i}(\Theta_s+\Psi)$$

$$=\frac{\partial}{\partial\eta}(\Psi-\Phi), \tag{2·40}$$

where η is the conformal time ($d\eta=dt/a(t)$), $x(\eta)$ is the spatial trajectory of a null geodesic, $\boldsymbol{\gamma}=d\boldsymbol{x}(\eta)/d\eta$ is the direction cosine of photon propagation, and Γ^i_{jk} are the connection coefficients with respect to γ_{ij}. Further Θ_s is the gauge-invariant brightness temperature perturbation on the shear free hypersurface (i.e., Newtonian gauge) and given by[19]

$$\Theta_s(\eta, \boldsymbol{x}, \boldsymbol{\gamma})\equiv\frac{1}{4}\epsilon_{cr}-\frac{1}{k}V(\eta)\left[\frac{a'}{a}\mathrm{Y}(\boldsymbol{x})+\gamma^i\mathrm{Y}(\boldsymbol{x})_{|i}\right]. \tag{2·41}$$

Integrating Eq. (2·40) along a null geodesic from present η_0 back to some arbitrary time η after decoupling, we obtain

$$\begin{aligned}\Theta_s(\eta_0, \boldsymbol{x}_0, \boldsymbol{\gamma})&=\Theta_s(\eta, \boldsymbol{x}(\eta), \boldsymbol{\gamma})+\Psi(\eta, \boldsymbol{x}(\eta))-\Psi(\eta_0, \boldsymbol{x}_0)\\&\quad+\int_\eta^{\eta_0}\frac{\partial}{\partial\eta'}(\Psi(\eta', \boldsymbol{x}(\eta'))-\Phi(\eta', \boldsymbol{x}(\eta'))d\eta'\\&=\Theta_s(\eta, \boldsymbol{x}(\eta), \boldsymbol{\gamma})+\Psi(\eta, \boldsymbol{x}(\eta))-\Psi(\eta_0, \boldsymbol{x}_0)\\&\quad+2\int_\eta^{\eta_0}\frac{\partial}{\partial\eta'}\Psi(\eta', \boldsymbol{x}(\eta'))d\eta',\end{aligned} \tag{2·42}$$

where $\boldsymbol{x}_0=\boldsymbol{x}(\eta_0)$ and the last equality follows from the perturbed Einstein equation, $\Phi=-\Psi$, which holds in a universe with negligible anisotropic pressure perturbations and is true in the universe after decoupling.

Although this formulation is perfectly correct, Θ_s given by Eq. (2·42) itself is not the anisotropy we observe. In fact, we observe the anisotropy on the matter rest frame on which we stand. The observable temperature anisotropy Θ_m on the matter rest frame is related with Θ_s as follows:[11),19)]

$$\Theta_m(\eta, \boldsymbol{x}, \boldsymbol{\gamma})=\Theta_s(\eta, \boldsymbol{x}, \boldsymbol{\gamma})+\frac{1}{k}\frac{a'}{a}V(\eta)\mathrm{Y}(\boldsymbol{x})+\frac{1}{k}V(\eta)\mathrm{Y}(\boldsymbol{x})_{|i}\gamma^i, \tag{2·43}$$

where a prime (′) represents $d/d\eta$.

From Eqs. (2·42) and (2·43), the present-day Θ_m is given by[15]

$$\Theta_m(\eta_0, \boldsymbol{x}_0, \boldsymbol{\gamma})=\Theta_{int}+\Theta_{sac}+\Theta_{dif};$$

$$\Theta_{int}\equiv\Theta_m(\eta, \boldsymbol{x}(\eta), \boldsymbol{\gamma})-\frac{1}{k}V(\eta)\mathrm{Y}(\boldsymbol{x}(\eta))_{|i}\gamma^i+\frac{1}{k}V(\eta_0)\mathrm{Y}(\boldsymbol{x}_0)_{|i}\gamma^i,$$

$$\Theta_{sac}\equiv\left(\Psi(\eta)\mathrm{Y}(\boldsymbol{x}(\eta))-\frac{1}{k}\frac{a'}{a}V(\eta)\mathrm{Y}(\boldsymbol{x}(\eta))\right)$$

$$-\left(\Psi(\eta_0)\mathrm{Y}(\boldsymbol{x}_0)-\frac{1}{k}\frac{a'}{a}V(\eta_0)\mathrm{Y}(\boldsymbol{x}_0)\right),$$

$$\Theta_{dif}\equiv 2\int_{\eta}^{\eta_0}\left(\frac{d}{d\eta'}\Psi(\eta')\right)\mathrm{Y}(\boldsymbol{x}(\eta'))d\eta'. \tag{2·44}$$

We note that we have $(a'/(ka))\,V=(2/3)\Psi=const$ in a flat matter dominated universe. Then Θ_{sac} reduces to the familiar Sachs-Wolfe effect,[6]

$$\Theta_{sac}=\frac{1}{3}\Psi(\eta)\mathrm{Y}(\boldsymbol{x}(\eta))-\frac{1}{3}\Psi(\eta_0)\mathrm{Y}(\boldsymbol{x}_0), \tag{2·45}$$

and Θ_{dif} vanishes. We call the term $\Theta_{GS}\equiv\Theta_{sac}+\Theta_{dif}$ the "generalized Sachs-Wolfe effect"[10] or Rees-Sciama effect in an open universe.

2.5. *Estimations of the present CMB anisotropy*

(a) Small scale anisotropy

First, we consider the small angular scale anisotropy of CMB.[11),19)] We find that the effect of the negative curvature and the effect due to Θ_{dif} on the small angle scale can be neglected. And moreover the monopole component of Θ_m is irrelevant to the anisortopies and for small angular scales the dipole component $(k^{-1}V\mathrm{Y}_{|i}\gamma^i$ evaluated at $\eta=\eta_0)$ is negligible. Thus in this case Eq. (2·44) can be reduced approximately to

$$\tilde{\Theta}_m(\eta_0,\boldsymbol{k},\gamma)\approx|\tilde{\Theta}_{int}(\eta,\boldsymbol{k},\gamma)+\tilde{\Theta}_{sac}(\eta,\boldsymbol{k},\gamma)|_{rms}e^{-ik\mu(\eta_0-\eta)}, \tag{2·46}$$

where $\tilde{\Theta}_m$, $\tilde{\Theta}_{int}$ and $\tilde{\Theta}_{sac}$ are the expansion coefficients of Θ_m, Θ_{int} and Θ_{sac} by the scalar harmonics with the eigenvalue k, respectively and $\mu\equiv(\boldsymbol{k}/|\boldsymbol{k}|)\cdot(\boldsymbol{\gamma}/|\boldsymbol{\gamma}|)=\hat{\boldsymbol{k}}\cdot\hat{\boldsymbol{\gamma}}$. And the subscript rms denotes the root-mean-square value of the quantity which is defined below.

Using Eq. (2·46), we can estimate the present small angle anisotropy of CMB as follows: The intrinsic temperature angular correlation function $C(\theta)$ is given by

$$C(\theta)/T_0^2=\langle\Theta_m(\eta_0,\boldsymbol{x},\hat{\boldsymbol{\gamma}})\cdot\Theta_m(\eta_0,\boldsymbol{x},\hat{\boldsymbol{\gamma}}')\rangle_{\boldsymbol{x}}$$

$$=\frac{1}{2\pi^2}\int_0^{\infty}\tilde{k}^2d\tilde{k}|\Theta(\tilde{k})|^2_{rms}\frac{\sqrt{-K}\sin(\tilde{k}r)}{\tilde{k}\sinh\sqrt{-K}r}, \tag{2·47}$$

where

$$r(\theta)=\frac{2}{\sqrt{-K}}\sinh^{-1}[\sinh\sqrt{-K}(\eta_0-\eta_{dec})\sin(\theta/2)], \tag{2·48}$$

T_0 is the present mean temperature of the CMB and

$$\tilde{k}=\sqrt{k^2+K}. \tag{2·49}$$

The quantity $\Theta(\tilde{k})$ is defined as

$$\Theta=\Theta_s(\eta_{dec},\hat{\boldsymbol{\gamma}})+\Psi(\eta_{dec}), \tag{2·50}$$

and its root-mean-square value is calculated as

$$|\Theta(\tilde{k})|^2_{rms}=\sum_{l=0}^{\infty}\frac{(\tilde{k}^2-K)\cdots(\tilde{k}^2-Kl^2)}{(2l+1)(\tilde{k}^2-K)^l}|\Theta_{(l)}(\eta_{dec})|^2\,. \tag{2·51}$$

In the actual observations, the intrinsic temperature correlation $C(\theta)$ cannot be directly obtained. Thus quantitative comparison of theory and observation is possible by taking into account the antenna response properly. The effect of the antenna beam width σ can be approximated by the following Gaussian distribution function:[9),10)]

$$f(|\boldsymbol{\gamma}_1-\boldsymbol{\gamma}_2|;\sigma)=\frac{1}{2\pi\sigma^2}\exp\left(-\frac{1}{2\sigma^2}|\boldsymbol{\gamma}_1-\boldsymbol{\gamma}_2|^2\right), \tag{2·52}$$

where $\boldsymbol{\gamma}_1$ and $\boldsymbol{\gamma}_2$ are direction cosines. Convolution of $C(\theta)$ with the above antenna beam function yields the angular correlation function $C(\theta;\sigma)$ of two measurements spaced an angle θ apart with an antenna of beam-size σ:

$$C(|\boldsymbol{\gamma}_1-\boldsymbol{\gamma}_2|;\sigma)=\int d\Omega_1' d\Omega_2' f(|\boldsymbol{\gamma}_1-\boldsymbol{\gamma}_1'|;\sigma)f(|\boldsymbol{\gamma}_2-\boldsymbol{\gamma}_2'|;\sigma)C(|\boldsymbol{\gamma}_1'-\boldsymbol{\gamma}_2'|)\,. \tag{2·53}$$

Here it must be noticed that the Gaussian beam size σ of an antenna is related to the beam size defined by FWHM, σ_{FWHM} as follows:

$$\sigma_{FWHM}=2\sqrt{2\ln 2}\,\sigma\,. \tag{2·54}$$

Under the small angle approximation, the above expression reduces to

$$\frac{C(\theta;\sigma)}{T_0^2}=\frac{1}{4\pi^2\sigma^2}\int_0^\infty \tilde{k}^2 d\tilde{k}|\Theta(\tilde{k})|^2 \times\int_0^\infty d\phi\frac{\sin(\tilde{k}\lambda_{dec}\phi)}{\tilde{k}\lambda_{dec}}\exp\left(-\frac{\theta^2+\phi^2}{4\sigma^2}\right)J_0\left(\frac{\phi^2}{2\sigma^2}\right), \tag{2·55}$$

where $\lambda_{dec}\equiv\eta_0-\eta_{dec}$. The observable temperature anisotropies, $\delta T/T(\theta,\sigma)$, are:

$$\begin{aligned}\left\langle\left|\frac{\delta T}{T}(\theta;\sigma)\right|^2\right\rangle &=\left(\frac{3}{2}C(0,\sigma)-2C(\theta;\sigma)+\frac{1}{2}C(2\theta;\sigma)\right)/T_0^2\\ &=\frac{1}{2\pi^2}\int_0^\infty \tilde{k}^2 d\tilde{k}|\Theta(\tilde{k})|^2\int_0^{(\pi/2)} du\,\sin u\,\exp(-\sigma^2\tilde{k}^2\lambda_{dec}^2\sin^2 u)\\ &\quad\times\left(\frac{3}{2}-2J_0(\theta\tilde{k}\lambda_{dec}\sin u)+\frac{1}{2}J_0(2\theta\tilde{k}\lambda_{dec}\sin u)\right)\end{aligned} \tag{2·56}$$

for triple beam switching experiments[23)~25)] and

$$\begin{aligned}\left\langle\left|\frac{\delta T}{T}(\theta;\sigma)\right|^2\right\rangle &=(2C(0,\sigma)-2C(\theta;\sigma))/T_0^2\\ &=\frac{1}{2\pi^2}\int_0^\infty \tilde{k}^2 d\tilde{k}|\Theta(\tilde{k})|^2\int_0^{(\pi/2)} du\,\sin u\,\exp(-\sigma^2\tilde{k}^2\lambda_{dec}^2\sin^2 u)\\ &\quad\times(2-2J_0(\theta\tilde{k}\lambda\sin u))\end{aligned} \tag{2·57}$$

for double beam switching experiments.[26),27)] The explanation about the beam switching will be shown in § 4.1. Using the above formula, we can estimate the predicted small-angle anisotropy $\delta T/T$ in any model.

(b) Large scale anisotropy

Now we turn to the large scale anisotropy of the CMB. In this case we have to derive the promised formula for multipole moments of the present CMB anisotropy while for the small-angle anisotropy we have to consider only the root mean square of the radiation perturbation. There has not appeared any work which considers an open universe model and includes both the generalized Sachs-Wolfe effect and intrinsic photon fluctuations at decoupling completely in evaluating the large scale anisotropy of the CMB, e.g., quadrupole moment of the CMB anisotropy. This unsatisfactory situation is mainly due to a technical difficulty in estimating the present quadrupole and/or higher multipoles of the CMB anisotropy in an open universe.[15] However, we have succeeded in deriving a formula by which one may calculate any multipole moment of the CMB anisotropy with particularly arbitrary precision.[15] We derive this formula below.

Instead of dealing directly with $P^{i_1\cdots i_l}_{(l)}$, for convenience, we introduce an operator G_l which acts on a harmonic function, defined as

$$G_l[\mathrm{Y}(\boldsymbol{x})]=(ik)^{-l}\mathrm{Y}_{|i_1\cdots i_l}(\boldsymbol{x})P^{i_1\cdots i_l}_{(l)}\,. \tag{2·58}$$

Then the temperature anisotropy Θ_m is expanded into multipole moments as

$$\Theta_m(\eta,\boldsymbol{x},\gamma)=\sum_{l=0}^{\infty} i^{-l}\theta_{m(l)}(\eta)G_l[\mathrm{Y}(\boldsymbol{x})]\,. \tag{2·59}$$

In the flat case $K=0$, $\mathrm{Y}=e^{i\boldsymbol{k}\cdot\boldsymbol{x}}$ and Eq. (2·59) reduces to the familiar representation,

$$\Theta_m(\eta,\boldsymbol{x},\gamma)=\sum_{l=0}^{\infty} i^{-l}\theta_{m(l)}(\eta)P_l(\hat{\boldsymbol{k}}\cdot\gamma)\exp(i\boldsymbol{k}\cdot\boldsymbol{x})\,,$$

where P_l is the l-th Legendre polynomial and $\hat{\boldsymbol{k}}\equiv\boldsymbol{k}/|\boldsymbol{k}|$.

What we need is a relation between different multipole moments at different times. The key property of a harmonic function for this purpose is

$$\mathrm{Y}(\eta)=\sum_{l=0}^{\infty}(2l+1)Z_\nu{}^l(\eta-\eta_0)G_l[\mathrm{Y}(\eta_0)]\,, \tag{2·60}$$

where $\mathrm{Y}(\eta)=\mathrm{Y}(\boldsymbol{x}(\eta))$ and $Z_\nu{}^l$ is defined by

$$Z_\nu{}^l(\eta-\eta_0)=i^{-l}X_\nu{}^l(\eta_0-\eta)\,,$$

$$X_\nu{}^l(\chi)=\left(\frac{\pi}{2\sinh(\sqrt{-K}\chi)}\right)^{1/2}(\nu^2+1)^{(l/2)}P^{-(l+1/2)}_{i\nu-1/2}(\cosh(\sqrt{-K}\chi))\,. \tag{2·61}$$

Note the change in the sign of the argument. The function $X_\nu{}^l(\chi)$ is the radial part of a harmonic function in the usual hyperspherical coordinates (χ,θ,φ) (see the Appendix of Ref. 15)) and ν represents an eigenvalue related to k as

$$\frac{k^2}{(-K)}=\nu^2+1\,. \tag{2·62}$$

Then, as shown in the Appendix of Ref. 15), provided G_l acts on $\mathrm{Y}(\eta)$ (i.e., a harmonic function along a null geodesic), G_l is expressed as a polynomial of degree

l in the ordinary derivative operator $\tilde{p}=(ik)^{-1}d/d\eta$ which satisfies the following recurrence relation,

$$G_0=1\,,\quad G_1=\tilde{p}\,,$$

$$G_{l+1}=\frac{2l+1}{l+1}\tilde{p}G_l-\frac{l}{l+1}\frac{\nu^2+l^2}{\nu^2+1}G_{l-1}\,. \tag{2·63}$$

Operating G_n on Eq. (2·60), we have

$$G_n(\tilde{p})\mathrm{Y}(\eta)=\sum_{l=0}^{\infty}(2l+1)G_n(\tilde{p})Z_\nu{}^l(\eta-\eta_0)G_l(\tilde{p}_0)\mathrm{Y}(\eta_0)\,, \tag{2·64}$$

where $\tilde{p}_0=(ik)^{-1}d/d\eta_0$.

With these formulas at hand, the present multipole moments $\theta_{m(l)}(\eta_0)$ are expressed from Eqs. (2·44) and (2·59) as follows:

For $l=0$ (monopole);

$$\theta_{m(0)}(\eta_0)=\sum_{n=0}^{\infty}i^{-n}\theta_{int(n)}(\eta)G_nZ_\nu{}^0(\Delta\eta)+\left(\Psi(\eta)-\frac{1}{k}\frac{a'}{a}V(\eta)\right)Z_\nu{}^0(\Delta\eta)$$
$$-\left(\Psi(\eta_0)-\frac{1}{k}\frac{a'}{a}V(\eta_0)\right)+2\int_\eta^{\eta_0}\left(\frac{d\Psi}{d\eta}\right)Z_\nu{}^0(\Delta\eta)d\eta\,, \tag{2·65}$$

where $\Delta\eta=\eta-\eta_0$ and

$$\theta_{int(n)}=\begin{cases}\theta_{m(1)}+V & \text{for}\quad n=1\,,\\ \theta_{m(n)} & \text{for}\quad n\neq 1\,.\end{cases}$$

For $l=1$ (dipole);

$$i^{-1}\theta_{m(1)}(\eta_0)=3\sum_{n=0}^{\infty}i^{-n}\theta_{int(n)}(\eta)G_nZ_\nu{}^1(\Delta\eta)+3\left(\Psi(\eta)-\frac{1}{k}\frac{a'}{a}V(\eta)\right)Z_\nu{}^1(\Delta\eta)$$
$$-i^{-1}V(\eta_0)+6\int_\eta^{\eta_0}\left(\frac{d\Psi}{d\eta}\right)Z_\nu{}^1(\Delta\eta)d\eta\,. \tag{2·66}$$

For $l\geq 2$ (quadrupole and higher multipoles);

$$i^{-l}\theta_{m(l)}(\eta_0)=(2l+1)\left[\sum_{n=0}^{\infty}i^{-n}\theta_{int(n)}(\eta)G_nZ_\nu{}^l(\Delta\eta)\right.$$
$$\left.+\left(\Psi(\eta)-\frac{1}{k}\frac{a'}{a}V(\eta)\right)Z_\nu{}^l(\Delta\eta)+2\int_\eta^{\eta_0}\left(\frac{d\Psi}{d\eta}\right)Z_\nu{}^l(\Delta\eta)d\eta\right]. \tag{2·67}$$

For a given l, in principle, the above formula can be used to evaluate the moment $\theta_{m(l)}$ by successive operation of G_n with $n=1, 2, 3, \cdots$ on the known function $Z_\nu{}^l$. However, in practice, it is a formidable task and this is the reason why no reliable work has been done so far. In what follows, we present a multipole moment formula which is practically tractable.

It can be shown that $Z_\nu{}^l$ has the property (see the Appendix of Ref. 15)),

$$\bar{p}Z_\nu{}^l=\frac{l}{2l+1}Z_\nu{}^{l-1}+\frac{l+1}{2l+1}\frac{\nu^2+(l+1)^2}{\nu^2+1}Z_\nu{}^{l+1}, \tag{2·68}$$

and that together with Eq. (2·63) it leads to the formula,

$$G_nZ_\nu{}^l=\frac{c_n}{c_l}G_lZ_\nu{}^n,\ ;\ c_n=\begin{cases}1 & \text{for}\quad n=0,\\ \prod_{j=1}^{n}\dfrac{\nu^2+j^2}{\nu^2+1} & \text{for}\quad n\geq 1,\end{cases} \tag{2·69}$$

for arbitrary non-negative integers n and l.

Since, given a specific l, it is straightforward to solve for G_l by using Eq. (2·63), the explicit expression for $G_lZ_\nu{}^n$ can be easily obtained next by using Eq. (2·68). As examples, we give the expressions for dipole and quadrupole:

(i) Dipole ($l=1$)

$$G_nZ_\nu{}^1=c_nG_1Z_\nu{}^n=c_n\bar{p}Z_\nu{}^n=\frac{n}{2n+1}c_nZ_\nu{}^{n-1}+\frac{n+1}{2n+1}c_{n+1}Z_\nu{}^{n+1}. \tag{2·70}$$

(ii) Quadrupole ($l=2$)

$$\begin{aligned}G_nZ_\nu{}^2&=\frac{c_n}{c_2}G_2Z_\nu{}^n=\frac{c_n}{c_2}\left(\frac{3}{2}\bar{p}^2-\frac{1}{2}\right)Z_\nu{}^n\\ &=\frac{3}{2}\frac{(n-1)n}{(2n-1)(2n+1)}q_nZ_\nu{}^{n-2}\\ &\quad+\left[\frac{3}{2}\frac{n^2}{(2n-1)(2n+1)}\frac{\nu^2+n^2}{\nu^2+1}q_n+\frac{3}{2}\frac{(n+1)^2}{(2n+1)(2n+3)}q_{n+1}-\frac{1}{2}\right]Z_\nu{}^n\\ &\quad+\frac{3}{2}\frac{(n+1)(n+2)}{(2n+1)(2n+3)}q_{n+2}Z_\nu{}^{n+2},\end{aligned} \tag{2·71}$$

where

$$q_n=\begin{cases}1 & \text{for}\quad n<3,\\ \prod_{j=3}^{n}\dfrac{\nu^2+j^2}{\nu^2+1} & \text{for}\quad n\geq 3.\end{cases}$$

Equations (2·66) and (2·70) give the desired formula for the dipole moment and Eqs. (2·67) with $l=2$ and (2·71) for the quadrupole moment.

Here we remark that in the flat universe ($K=0$), G_n reduces to the Legendre polynomial P_n and $Z_\nu{}^l(\eta)$ to i^n times the spherical Bessel function $i^lj_l(k\eta)$. Following the above formula, we can estimate the expected anisotropy of CMB in any model.

2.6. *Initial condition of perturbations*

Here the initial conditions on the evolution of small fluctuations are shown. Though the real initial conditions are concerned with the detailed mechanism of creation of fluctuations such as the inflation, we can classify the set of the solution for the evolution of fluctuations in the very early universe. Hence we only have to set up some initial conditions at radiation dominated era. We take this epoch at the photon

temperature $T=10^8$ K after occurring the e^+e^- annihilation. Then we can get approximately analytic two independent growing mode solutions at this early stage in the evolution equations. Physically, they correspond to the adiabatic and the isocurvature condition. We show here the relation between those initial conditions and the entropy perturbation. In the early universe, the cosmological entropy is dominated by the radiation and the universe is in the radiative equlibrium. Then we can neglect the intrinsic entropy of the matter other than radiation and the entropy perturbation S_{mr} becomes

$$S_{mr}\equiv\frac{\delta(n_m/s)}{(n_m/s)}=\frac{\delta n_m}{n_m}-\frac{\delta_s}{s}=\frac{\Delta_{cm}}{1+w_m}-\frac{\Delta_{cr}}{1+w_r}, \tag{2·72}$$

where the suffix m stands for matter, i.e., baryon or other nonbaryonic dark matter particles if there exist, r for radiation and $s=(4a^3/3T)\rho_r$ is the entropy density of radiation. As for the adiabatic condition, we set $S_{mr}=0$ for all matter components. The growing mode solution of the total density perturbation Δ is proportional to a^2. As for the isocurvature initial condition, S_{mr} is set to a constant in time for one matter component. The growing mode solution is $\Delta\propto a^3$.[22] It is noted that the entropy perturbations of other matter components become negligibly small. In order to know the geometrical meaning of these conditions, we show the curvature perturbation. The curvature perturbation Φ is concerned with Δ through the Poisson equation (2·17). If we take the adiabatic initial condition, the term on the right-hand side of Eq. (2·18) becomes constant because $\rho\propto a^{-4}$ in the early universe. Hence Φ becomes constant in time. On the other hand, if the isocurvature initial condition is taken, $\Phi\propto a$ and is negligible small in the early epoch. So this type of initial condition is called isocurvature.

The power spectrum of the total density perturbation is usually assumed the power-law form. We define the power law index as follows:

$$|\Delta|^2\propto\tilde{k}^n, \tag{2·73}$$

where $\tilde{k}^2\equiv k^2+K$. In particular, the spectrum with $n=1$ for both adiabatic and isocurvature fluctuations becomes scale free. This is known as Harrison-Zeldovich spectrum and naturally obtained by the inflationary scenario.[46] It should be noticed that our power index differs by 4 from that used by, e.g., Peebles[12] for isocurvature perturbations (i.e., $n=n_{\text{Peebles}}+4$) because his definition of index is the power-law index of the entropy perturbation.

2.7. *Normalization of density perturbations*

Finally, we summarize the procedure how the CMB anisotropy in any model can be estimated and how we can give constraint on the models: For any model we can get the present perturbations numerically by the method which we described before. However since our analysis in the present paper is carried out in the framework of linear theory, consideration of its cosmological consequences requires an appropriate normalization method based on a reliable quantitative measure of the present cosmological structures *in its linear regime*. Usually, before the discovery of the large-angle anisotropy of the CMB by *COBE* (see § 4. 2), the conventional method uses the

galaxy-galaxy correlation function $\xi(r)$[9),19)] or its volume integral, $J_3(r)$:[19),29)] According to linear theory, they are calculated as follows:[10)]

$$\xi(r)=\frac{1}{2\pi^2}\int_0^\infty \tilde{k}^2 d\tilde{k} P(\tilde{k})\frac{\sqrt{-K}\sin(\tilde{k}r)}{\tilde{k}\sinh\sqrt{-K}r}, \tag{2·74}$$

where $\tilde{k}$ is defined in Eq. (2·49) and $P(\tilde{k})\equiv|\Delta_{cm}(\tilde{k})|^2$ is the fluctuation power spectrum at the present time. The volume integral of $\xi(r)$ gives $J_3(r)$:

$$J_3(r)\equiv\int_0^r \xi(x)x^2dx=\frac{1}{2\pi^2}\int_0^\infty d\tilde{k}P(\tilde{k})\frac{\sin\tilde{k}r-\tilde{k}r\cos\tilde{k}r}{\tilde{k}}. \tag{2·75}$$

Furthermore, we often use the normalization condition that the mass excess $\delta M/M$ within te radius $r=8h^{-1}$ Mpc, equals 1.0. Although the above quantities have well-established values from an observational point of view,[30)~32)] a normalization procedure based on either of them necessarily assumes that galaxies trace the mass distribution of the universe, which may not be the case in reality.[33)~35)]

A way out of this is to use the large-scale peculiar velocity field which should measure the *dynamical* mass distribution. The rms peculiar velocity field with a Gaussian window function[36)] can be expressed as

$$v_{rms}^2(r)=\frac{\Omega^{1.2}H_0^2}{2\pi^2}\int_0^\infty P(\tilde{k})\exp(-\tilde{k}^2r^2)d\tilde{k}, \tag{2·76}$$

while the velocity correlation function[17),37)] is

$$v_{cor}^2(r)=\frac{\Omega^{1.2}H_0^2}{2\pi^2}\int_0^\infty d\tilde{k}P(\tilde{k})\frac{\sin\tilde{k}r}{\tilde{k}r}, \tag{2·77}$$

where $H_0\equiv100\,h$km/sec/Mpc is Hubble's constant. The normalization based on either Eq. (2·76) or (2·77) provides a potentially promising method since it does not require any assumption about the connection between luminous objects and the underlying actual mass distributions.[38)~40)] Unfortunately the present observational data are still controversial[41)~45)] and do not yet provide a reliable measure for normalization.

Using the power spectrum of matter perturbations obtained from the numerical integration, we found that the overall normalization factor is sensitive to the linear scale where the normalization is performed. This reflects the principal difficulty in comparing observations with linear theory predictions; on small scales where observational data are reliable, nonlinear effects should contaminate the linear results to some extent, while on large scales where nonlinear contamination is negligible, the observational uncertainties become large. Conventionally compromise has been made around at $r\sim10h^{-1}$ Mpc where ξ is of order unity, since beyond this length scale the observational data become rather uncertain.

From the above facts, different normalization schemes in which we use the different qualitative measures give the different amplitude[19),20)] and so the ambiguity of the normalization exists. However at last *COBE* has detected the intrinsic Gaussian temperature fluctuation of the CMB smoothed on 10°, σ_{sky} (10°)[3)] shown in

§ 4.2. Here we can obtain expected values of the CMB fluctuations directly from the observational data σ_{sky} (10°) of *COBE*. We normalize the amplitudes of the temperature fluctuations by coinciding the expected σ_{sky} (10°) with the observed one by *COBE*. Using this new normalization scheme, there is no biasing problem that is whether galaxies trace the mass or not.

Once $P(\tilde{k})=P(\tilde{k}, z=0)$ is normalized according to the above procedures, the power spectrum of matters at decoupling z_{dec} is calculated for $\Omega=1$:

$$P(\tilde{k}, z_{dec})=(1+z_{dec})^{-2}P(\tilde{k}) \tag{2·78}$$

and for $\Omega<1$:

$$P(\tilde{k}, z_{dec})=\left[\frac{(\cosh\sqrt{-K}\eta_0-1)^3}{(\cosh\sqrt{-K}\eta_0-1)(\cosh\sqrt{-K}\eta_0+5)-3\sqrt{-K}\eta_0\sinh\sqrt{-K}\eta_0}\right]^2 \times\frac{P(\tilde{k})}{25(1+z_{dec})^2} \tag{2·79}$$

(see Eqs. (2·37) and (2·38)). Since the relative amplitudes of photon to matter perturbations are calculated in linear theory, Eqs. (2·78) and (2·79) finally fix the amplitude of matter and photon perturbations at decoupling. Then the present amplitudes of matter perturbations and the temperature fluctuation on any scale are obtained as we described before. And by comparing the expected anisotropy on any angle scale and the matter fluctuations at the present time in a model with the results of the observations, we can constraint on the model as we will show in detail in § 4.

§ 3. Models

In this section, we show the models which we consider in this paper. We review the characters of the time evolution of density perturbations and the features of the resultant power spectra in the models, which are numerically estimated by the method presented in § 2.

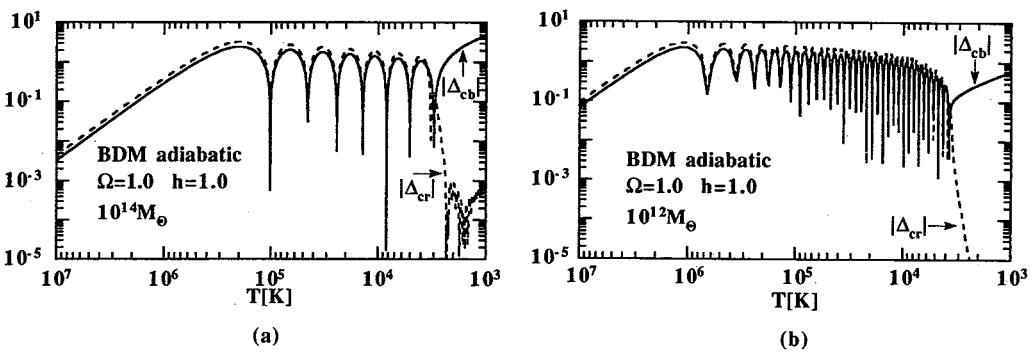

Fig. 1.(a) The time evolution of baryon and photon density fluctuations, Δ_{cb} and Δ_{cr} for adiabatic BDMs with mass scale $M=10^{14}M_\odot$. Temperature is that of radiation temperature and $\Omega_0=\Omega_b=h=1.0$. Normalization is arbitrary.
(b) The same as Fig. 1 (a), but with mass scale $M=10^{12}M_\odot$.

3.1. *Pure baryonic model*[11]

First of all, we consider the pure baryonic model. In this model, the universe contains only baryon and photon (then a-component is baryons; $a=b$ and photon; $a=r$) and at the present time the baryon dominated in the universe.

First, we consider the time evolution of initially adiabatic perturbations. As is well known, perturbations with mass scales greater than the Jeans mass M_J (M_J at the decoupling time is nearly $1.1\times10^{16}(\Omega_0h^2)^{-2}M_\odot$, where Ω_0 is the density parameter at present (in this model $\Omega_0=\Omega_b$)) and h is Hubble constant in units of 100 km s^{-1}Mpc^{-1}, grows as a^2 in the radiation-dominated stage and as a in the baryon-dominated stage.[22] On the other hand, for perturbations with scales smaller than the Jeans mass, the amplitude oscillates. Among them, those with scales larger than a critical mass $M_c(t)$ ($<M_J$) are damped gradually due to "adiabatic damping", in proportional to $a^{-1/4}$ at the baryon-dominated stage. However those with scales smaller than M_c are damped exponentially.

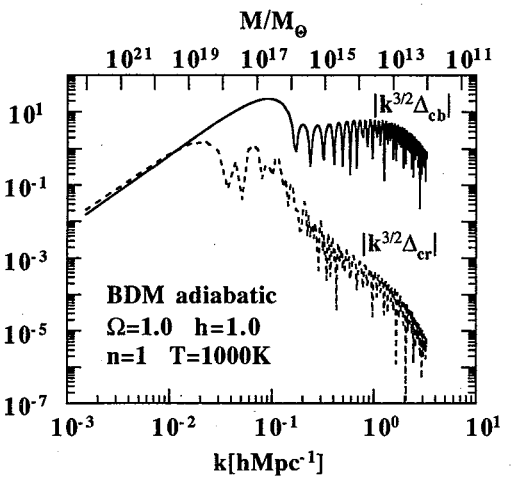

Fig. 2. The spectra of baryon and photon density fluctuations, Δ_{cb} and Δ_{cr} at $T=1000$ K for adiabatic BDMs with $\Omega_0=\Omega_b=h=1.0$ and $n=1$. Normalization is arbitrary.

At the stage before recombination when the fluid approximation is good, the analytic estimate of M_c was done by Silk,[47] Sato[48] and Weinberg,[49] yielding the damping factor as $\exp(-(M_c/M)^{2/3})$ with $M_c\sim10^{11}\,M_\odot$ at $T=4000$ K. This is in good agreement with our numerical results. We show in Figs. 1(a) and (b) the time evolution of density fluctuations with the mass scales $M=10^{14}M_\odot$ and $M=10^{12}M_\odot$. We can see that as for $M=10^{14}M_\odot$ the baryon density fluctuation oscillates after when it enters the Jeans scale and after the decoupling it grows freely. As for $M=10^{12}M_\odot$, we can see

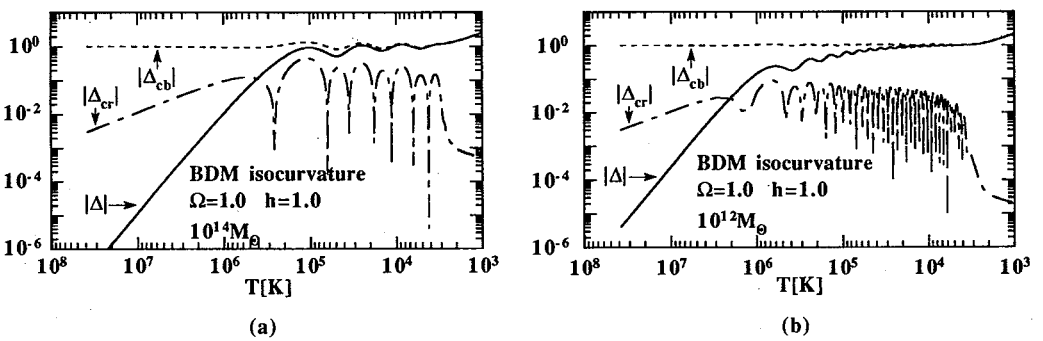

Fig. 3.(a) The time evolution of total, baryon and photon density fluctuations, Δ, Δ_{cb} and Δ_{cr} for isocurvature BDMs with mass scale $M=10^{14}M_\odot$. Temperature is that of radiation temperature and $\Omega_0=\Omega_b=h=1.0$. Normalization is arbitrary.
(b) The same as Fig. 3(a), but for isocurvature BDMs with mass scale $M=10^{12}M_\odot$.

well that the baryon density fluctuation damps exponentially during the recombination. Figure 2 shows the spectra of baryon and radiation fluctuations just after the decoupling era ($T=1000$ K). One can see the so-called "Silk-damping" below the "Silk-mass" $M_s \equiv M_c(t_D) \simeq 10^{13}\Omega_0^{1/4}\Omega_b^{-3/2}M_\odot$, where t_D is the decoupling time. The amplitude of perturbations just above Silk-mass increases slightly due to weak "velocity-overshoot effect", which results from decoupling of baryons from photons. For a small value of $\Omega_0 h^2$, M_s is larger and the amplitude of the prominent peak on the large-scale side decreases.

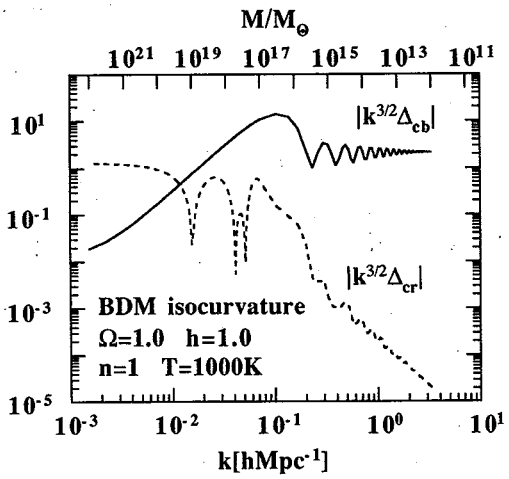

Fig. 4. The same as Fig. 2, but for isocurvature BDMs.

Second, we consider initially isocurvature perturbations. The behavior is quite different from that of initially adiabatic perturbations.[22] The baryon density perturbation Δ_{cb} with a mass scale larger than $M_J(\simeq 10^{16}\,M_\odot)$ decreases once in baryon-dominated stage and then starts to grow again atter decoupling. On the other hand, Δ_{cb} with a mass scale less than M_J oscillates around a constant value which is equal to the initial value of the entropy perturbation S_{br} after entering the horizon. These features are in agreement with analytic estimates and show that growing adiabatic modes are generated both on large-scales and small-scales. In particular, the amplitude of photon perturbations on large-scales grows significantly after the equal time. The time evolutions for $M=10^{12}\,M_\odot$ and $M=10^{14}M_\odot$ and the spectrum of density fluctuations in this case are shown in Figs. 3(a), 3(b) and 4, respectively. As for the time evolution of the isocurvature density fluctuation, we can see that the baryon density fluctuation does not damp exponentially even for the case that $M=10^{12}\,M_\odot$.

3.2. *Peebles' model*

Peebles[12),37] noted that possible reionization in his minimal isocurvature model would diminish the residual anisotropies on small scales. As a matter of fact, the origin of reionization is difficult to specify; in the pure baryonic models, one realistic source of ionizing photons would be the first nonlinear objects on small scales, such as Pop. III starts, which might appear in the isocurvature models with initially high power spectrum such as $n \gtrsim 3$. In the adiabatic models, such small objects cannot form because of Silk damping before decoupling (see Fig. 2). Although there is no specific model of the reionization, it is interesting to calculate the extent to which the CMB anisotropies in the isocurvature pure baryonic models would be diminished. The epoch of the reionization should be early enough, otherwise the universe would not become optically thick even if the ionization rate x_e were unity.[40]

We attempted to examine the effect of reionization as follows: We traced the evolution of baryons and photons in isocurvature models until $z=20$ on the basis of

the formulation described by equations in § 2. The ionization rate x_e was artificially fixed to unity until that time. Strictly speaking, this approach does not correspond to *reionization;* rather it describes the situation in which the last scattering surface of baryons and photons is moved from $z\sim1000$ to $z\sim20$. Thus this is an extreme case; we have maximized the effects of reionization.[19]

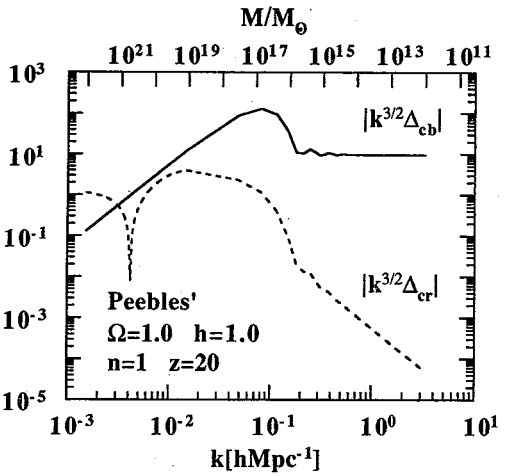

Fig. 5. The same as Fig. 4, but for Peebles' model at $z=20$.

The evolution of perturbations in this model is similar with that in the case that the coupling of baryon and photon is not so weak in the pure baryonic model. However the difference of the decoupling time results in the larger scale of the last scattering and then the larger smoothing of photon fluctuations on small-scales. The power spectrum at the $z=20$ is shown in Fig. 5. However, Ostriker and Vishiniac[50] and Vishiniac[51] have pointed out that significant small scale anisotropy can develop from quadratic non-linearities in the scattering which do not suffer from destructive interference, as different wave-modes are coupled. This effect is called "Vishiniac effect" and we discuss about this effect later (see in § 5.3 (c)).

3.3. *Cold dark matter model*[20]

Here, we consider cold dark matter (CDM) dominated universe model. In this model, the universe contains photon, baryon, CDM and massless neutrinos. The suffices α are r, b, x and n, respectively. Generally speaking, the density perturbation of CDM is continuously growing in time and the density perturbation of baryon is suddenly growing after decoupling gravitationally attracted by that of CDM even if it entered the Jeans scale before decoupling. Hence there exists no special scale in the spectrum of matter density fluctuations. The only scale shown in the CDM spectrum is the horizon scale of the matter radiation equal time, $L_{eq}=10(\Omega h^2)^{-1}$ Mpc. The growth of density perturbations is held down if the perturbations enter the horizon in the radiation dominated era. This suppression is known as *stagspansion.* In the spectrum, then we show mild bend at this horizon scale. Detailed evolutions of perturbations for the case of adiabatic and isocurvature initial perturbations are shown as follows.

For the case of adiabatic initial condition, the evolution of density perturbations is proportional to a^2 in a radiation dominant era, and to a in a matter dominant stage on the scale which is larger than the Jeans scale λ_J of the baryon and photon system. Once the scale becomes smaller than λ_J, Δ_{cb}, Δ_{cr} (and Δ_{cn}) begin to oscillate as acoustic waves and the growth of Δ_{cx} is suppressed in a radiation dominant era, i.e., stagspansion. As baryons recombine, the photo-diffusion takes place and if cold particles did not exist, Δ_{cb}, Δ_{cr} would damp. However because of the existence of cold particles,

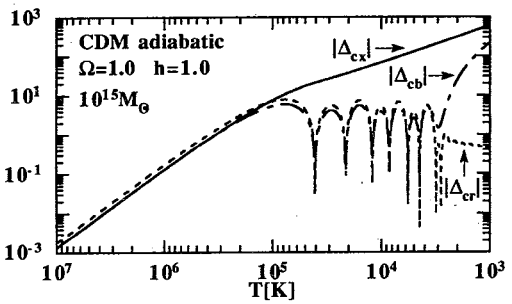

Fig. 6. The time evolution of CDM, baryon and photon density fluctuations, Δ_{cx}, Δ_{cb} and Δ_{cr} for aidabatic CDMs with $\Omega_0=h=1.0$ and mass scale $M=10^{15}M_\odot$. Normalization is arbitrary.

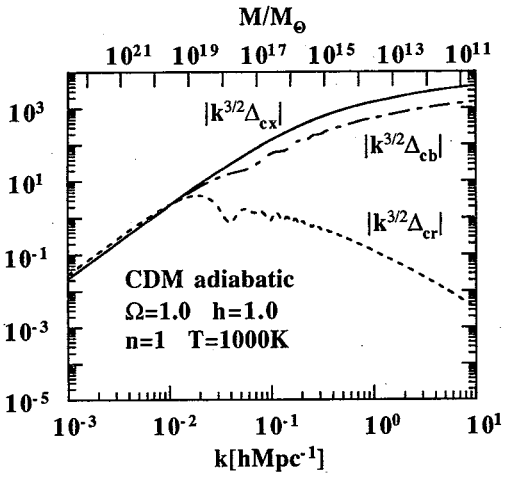

Fig. 7. The spectra of CDM, baryon and photon density fluctuations, Δ_{cx}, Δ_{cb} and Δ_{cr} at $T=1000$ K for aidabatic CDMs with $\Omega_0=h=1.0$ and $n=1$. Normalization is arbitrary.

Δ_{cb} begins to catch up with Δ_{cx} as soon as the coupling between baryons and photons is enough weak. These behaviors of the time evolution of the density fluctuations are shown in Fig. 6. The spectra of Δ_{cx}, Δ_{cr} and Δ_{cb} for this case at 1000 K with initially Harrison-Zeldovich spectrum are shown in Fig. 7. At this temperature, Δ_{cb} is almost close to Δ_{cx} and we can get the present spectrum of the total density perturbation Δ using analytic solutions as mentioned in § 2.

Next we consider the behavior of initially isocurvature perturbations. But the behavior is quite different which isocurvature condition is taken. As shown in § 2.6 the isocurvature condition is $S_{\alpha r}$ =const. In the CDM dominated model, we can choose α as either CDM or baryon. We call the former the axionic isocurvature condition because such condition is naturally realized when the axion plays a role of the dark matter. And the latter is called the baryonic isocurvature condition.

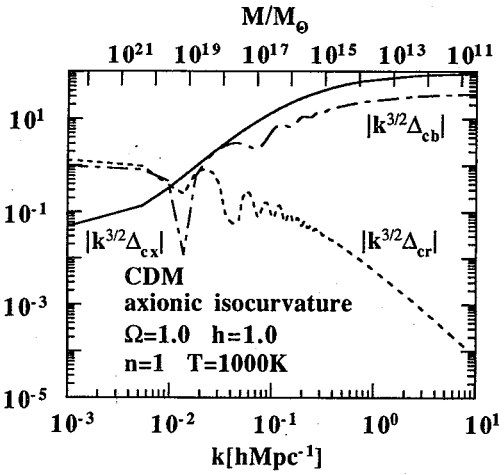

Fig. 8. The same as Fig. 7, but for axionic isocurvature CDMs at $T=1000$K.

As for the axionic isocurvature condition, the amplitude of density perturbation of CDM Δ_{cx} is initially positive constant and other components of perturbations are approximately zero. For example, the photon density perturbation Δ_{cr} is factor a_{eq}/a_i smaller than Δ_{cx}, where a_{eq} and a_i is the scale factor at matter radiation equal time and at the initial time, respectivelly. On the scale larger than Jeans scale λ_J, Δ_{cx} stays constant and other components approach negative constant modes. However, once the scale becomes smaller than λ_J, Δ_{cr} and Δ_{cn} begin to oscillate. Then Δ_{cx} becomes growing and Δ_{cb} starts catching up with Δ_{cx} in order to switch over adiabatic growing mode. The power spectrum of perturbations at 1000 K is shown in Fig. 8.

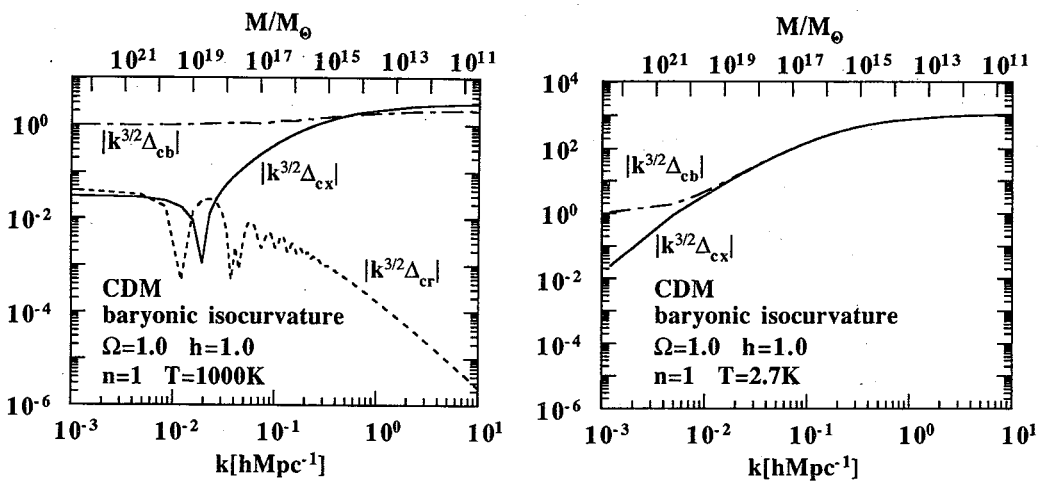

Fig. 9.(a) The same as Fig. 7, but for baryonic isocurvature CDMs at $T=1000$K.
(b) The same as Fig. 9(a), but at $T=2.7$ K.

As for baryonic isocurvature condition, you only have to exchange Δ_{cx} for Δ_{cb}. After entering the Jeans scale, however, the situation becomes different. Though Δ_{cx} starts growing to catch up with Δ_{cb}, it takes a long time for the models $\Omega_b < \Omega_x$. In Figs. 9(a) and (b), the power spectrum of perturbations at 1000 K and 2.7 K are shown. We find very different features between these two figures. In this paper, we only concentrate our attention on the axionic isocurvature condition.

As for CDM models, the most important difference between the spectrum of the isocurvature initial condition with that of adiabatic one is the existence of the large amplitude photon density perturbation on the large scale for isocurvature perturbations. This is the remnant of the initial condition. Then the expectation values of CMB anisotropies of isocurvature models on large scale become larger than those of adiabatic models.

3.4. *Hot dark matter model*[21),52)]

As well known, the candidate of hot dark matter (HDM) is massive neutrino. Since neutrino connects with baryon through the weak interaction, the decoupling time of neutrino is rather late in the history of the universe and it has large kinetic energy. Before the perturbations enter the neutrino Jeans scale, the behavior of evolution of perturbations is the same as the CDM model for both adiabatic and isocurvature initial conditions. When the density perturbation of HDM enters the Jeans scale, it is damped away by the free streaming. The Jeans scale is comparable to the horizon scale when the photon temperature is enough higher than the neutrino rest mass. As the temperature drops under the neutrino mass, the Jeans scale suddenly decreases because the neutrino begins to behave as a non-relativistic particle. Hence the largest Jeans scale $\lambda_{\rm Max}$ is that at the temperature of neutrino mass. It is expressed as

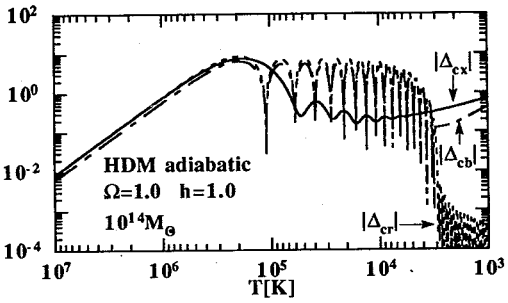

Fig. 10. The time evolution of HDM, baryon and photon density fluctuations, Δ_{cx}, Δ_{cb} and Δ_{cr} for adiabatic HDMs with $\Omega_0=h=1.0$ and mass scale $M=10^{14}M_\odot$. Normalization is arbitrary.

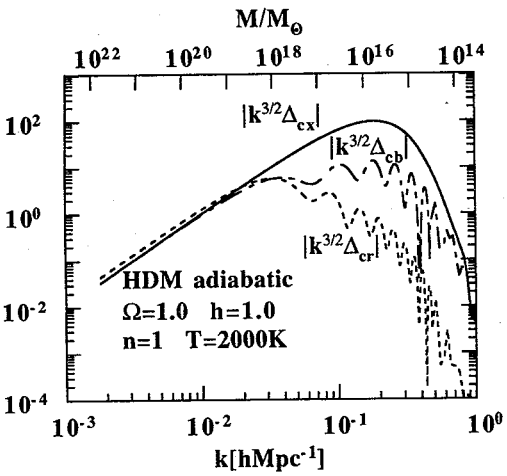

Fig. 11. The spectra of HDM, baryon and photon density fluctuations, Δ_{cx}, Δ_{cb} and Δ_{cr} at $T=2000$ K for adiabatic HDMs with $\Omega_0=h=1.0$ and $n=1$.

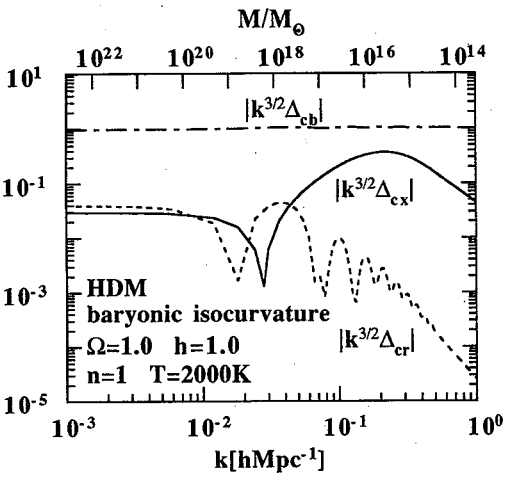

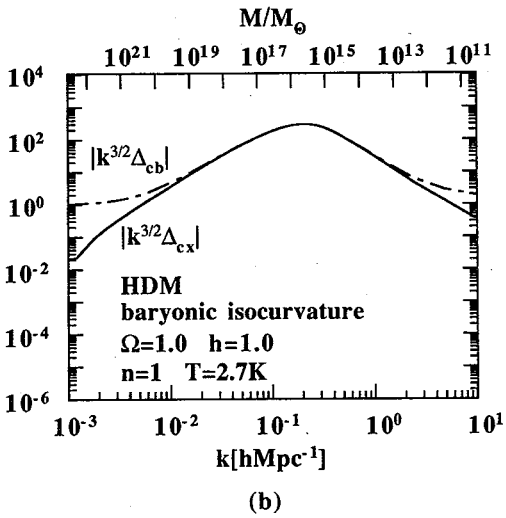

Fig. 12.(a) The same as Fig. 11, but for baryonic isocurvature HDMs at $T=2000$ K.
(b) The same as Fig. 12(a), but at $T=2.7$K.

$$\lambda_{\mathrm{Max}}=12\frac{N}{\sqrt{1+0.27N}}(\Omega h^2)^{-1}\ \mathrm{Mpc}\,, \tag{3·1}$$

where N is the number of massive Dirac neutrino species. This scale gives us the peak of the spectrum. We show the time evolution of density fluctuations for HDMs in Fig. 10. In Fig. 11, the spectrum for adiabatic condition at $T=2000$ K is shown. Figures 12(a) and (b) show the spectra for isocurvature conditions and the temperature are 2000 K and 2.7 K, respectively. As for adiabatic perturbations, however, the density perturbations grow according to the analytic solution (Eqs. (2·78) and (2·79)) and the HDM spectrum does not change their shape till the present. As for isocurvature perturbations, we take the baryonic isocurvature initial condition since only baryon can be treated as dust before HDM decouples. And it should be noted that

there exist not only the large scale perturbations of baryon and photon, but also the small scale perturbations of baryon and neutrino. This existence of small scale perturbations may become one of the advantage of the isocurvature condition because this may directly produce the small scale structures.

3.5. *Effects of the cosmological constant on CMB anisotropies*[38),53)]

Here, we investigate effects of the positive cosmological constant on CMB anisotropies. Since the cosmological constant plays an important role only at late epochs, the evolution of density perturbations is not influenced by it before the universe becomes optically thin. Hence the cosmological constant does not affect physical processes before recombination such as Silk damping. There are two main effects of the cosmological constant. One is the change in the growth factor of the total matter perturbation Δ from the recombination to the present.[54)] The other is a modification of the temperature correlation due to the change of the curvature scale. In what follows, we consider only the totally flat universe, that is, $\Omega_0+\lambda=1.0$, where $\lambda\equiv\Lambda/3H_0^2$. Let us estimate these two effects separately.

In an open universe, the growth of matter density perturbation is suppressed after the redshift of $z\simeq 1/\Omega_0-2$ due to the curvature effect. On the other hand, the suppression occurs at a later stage $z\simeq(1/\Omega_0-1)^{1/3}-1$ in the flat universe with the cosmological constant. As a result, the growth factor of the latter becomes larger than that of the former. The growing mode solution in the matter dominated stage is obtained by an integral form as[17)]

$$\Delta\propto H\int da/(Ha)^3\,. \tag{3·2}$$

We show the growth factor $\Delta(T=2.7\,\mathrm{K})/\Delta(T=1000\,\mathrm{K})$ compared with that in models without the cosmological constant in Fig. 13. We found that, for example, the growth factor of a low density model with $\Omega_0=0.1$ and $\lambda=0.9$ is about 300 % greater than the corresponding model without the cosmological constant. This effect directly affects

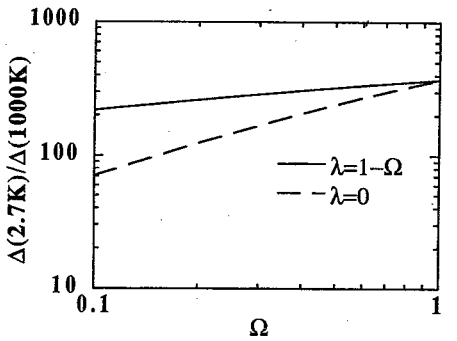

Fig. 13. The growth factor of the total density perturbations from 1000 K to 2.7 K as a function of Ω_0. The solid line and the dashed line represent the growth factor for the universe with and without the cosmological constant, respectively.

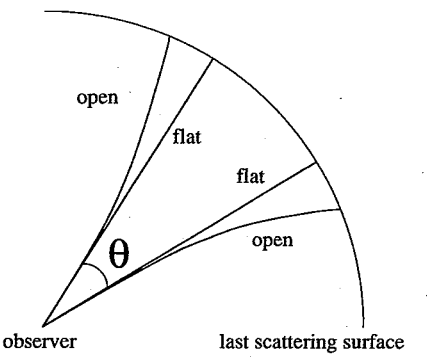

Fig. 14. Light path from the last scattering surface corresponding to an observational angle θ in the spatially flat and open geometry.

the normalization of the perturbation variables and reduces CMB anisotropies.

The modification of the temperature correlation occurs as follows. As shown in § 2.4, using the small angle approximation, the intrinsic temperature correlation function is obtained (Eq. (2·47))

$$C(\theta)/T_0^2 = \left\langle \frac{\delta T}{T}(\boldsymbol{\gamma}) \frac{\delta T}{T}(\boldsymbol{\gamma}') \right\rangle$$

$$= \frac{1}{2\pi^2} \int dk k^2 |\Theta(k)|^2_{rms} \frac{\sin \alpha k\theta}{\alpha k\theta}, \tag{3·3}$$

where $\mu \equiv \boldsymbol{k}\cdot\boldsymbol{\gamma}/k$, $\theta = |\boldsymbol{\gamma} - \boldsymbol{\gamma}'|$ and $\Theta(k)$ is the gauge invariant brightness function for the matter rest frame. For a flat universe, $\alpha \equiv \eta_0 - \eta_d$ where η_d is the conformal time at photon radiation decoupling. On the other hand, for an open universe model $\alpha \simeq (-K)^{-1/2} \sinh[(-K)^{1/2}(\eta_0 - \eta_d)]$ for a small angular separation with K given by $K = -a^2 H(1-\Omega)$. The CMB anisotropy at an observational angle θ is essentially the difference between temperatures in two points separated by $\alpha\theta$ on the last scattering surface. The difference, i.e., the CMB anisotropy increases as we see farther separated points. The curvature term works to enlarge the separation for a given observational angle θ as shown in Fig. 14. Conversely the absence of the curvature term reduces the CMB anisotropy at a given angle because we see narrower and more strongly correlated points.

Thus both of the two effects work to reduce the CMB anisotropy $\delta T/T$. As a result, the expected values of temperature fluctuations in the low density but flat universe with cosmological constant are smaller than those without cosmological constant.

§ 4. Constraint on the galaxy formation models

4.1. *Observations of CMB anisotropies before COBE*

The important observations on CMB anisotropy before the results of the *COBE* group are briefly summarized.

In order to realize the high degree of accuracy, beam switching experiments are usually adopted instead of direct measurements of black body temperature in each sky position. The temperature difference between two antennas separated by an angle θ or three antennas by θ and 2θ is measured. Each observation has a different antenna beam width σ. The temperature anisotropies of double and triple beam are $\Delta T/T \equiv \langle (T_1 - T_2)^2 \rangle^{1/2}/T$ and $\Delta T/T \equiv \langle [T_0 - (T_1 - T_2)/2]^2 \rangle^{1/2}/T$, respectively. Here, T_1 and T_2 is the temperature of the two beams separated by angle θ for the double beam experiment. As for the triple beam experiment, T_0 is the temperature of the central beam and T_1 and T_2 are the temperature of beams displaced by an angle θ to either side of the central beam.

Many observations have done and covered a wide range of angular scale from a few arcseconds to the dipole anisotropy. The typical scale of observed galaxies and the large scale structures of the universe correspond to several arcminutes and a few degrees. So the observations on these scales are very important for structure forma-

tions.

The most severe limit on small scale has been obtained by Readhead et al.[25] It is a triple beam experiment and their upper limit of the temperature anisotropy, the angular scale and gaussian beam width are

$$\frac{\delta T}{T}<2.1\times10^{-5}, \quad \theta=7.'15, \quad \sigma=0.'77. \tag{4·1}$$

On the intermediate scale, the result by Meinhold and Rubin[27] is the most important. Though their measurement is a double beam experiment, the scale is nearly equal the horizon scale at matter radiation equal time. So expected anisotropies of cosmological models take the peak value around this scale. Their limit, angular scale and beam width are

$$\frac{\delta T}{T}<3.5\times10^{-5}, \quad \theta=1^{\circ}, \quad \sigma=13'. \tag{4·2}$$

On the large scale, severe bounds are obtained by Watson et al.:[55]

$$\frac{\delta T}{T}<1.8\times10^{-5}, \quad \theta=5^{\circ}, \quad \sigma=2^{\circ}. \tag{4·3}$$

Meyer et al.[56] made the sky map of microwave though they could not find the intrinsic temperature fluctuations. Hence they could obtain the correlation function $C(\theta)$ itself. The upper limit by fitting the correlation function to the Gaussian form is 1.6×10^{-5} at correlation angle of 13°. Between 3° to 22°, the upper limit of fluctuations is 4.0×10^{-5}.

But now, real temperature anisotropies have been obtained by the *COBE* group on the scale larger than a few degrees. And the upper limits by Watson et al. and Meyer et al. are larger than the *COBE*'s data. We will show the *COBE*'s results in the next subsection.

4.2. *Observations by COBE*[3]

Finally, the DMR(Differential Microwave Radiometer) instrument of *COBE* has found CMB anisotropies. The DMR experiment[57),58] is one of three complementary experiments to be flown on the *COBE* mission. The satellite has three DMRs which operate at frequencies: 31.5, 53 and 90 GHz in order to remove Galactic emission whose strength depends on frequencies. Those three frequencies are chosen to be near the minimum in Galactic emission and near the CMB maximum. Each instrument contains one pair of (31.5 GHz) or two pairs of (53 and 90 GHz) horn antenna. The angle between two antennas of each pair is 60°. The temperature difference between these two directions can be obtained. The beam width of each antenna is 7° FWHM. It is practicable to remove the instrumental noise by comparing two independent channels at each frequency. And the combined motions of spacecraft spin (75 s period), orbit (103 minute period) and orbital precession (~1 degree per day) allow each sky position to be compared to all others through a massively redundant set of all possible difference measurements spaced 60° apart. After all, *COBE* group has made all the sky maps of temperature by analyzing the first year of data. And

the data are fitted to spherical harmonic expansions and sky maps with 6144 nearly equal area pixels (2.°6×2.°6) using the least-squares minimization and a sparse matrix technique.

The dipole anisotropy is dominated in the DMR maps. The temperature amplitude ΔT is 3.36±0.1 mK and the direction is $l=264.7\pm0.8$, $b=48.2\pm0.5$. It is believed that this dipole anisotropy is produced by our peculiar motion relative to the CMB rest frame. The doppler velocity of solar system is $v\simeq c\Delta T/T=370$ km/s.

After removing dipole and kinematic quadrupole, no obvious features are shown away from the Galactic plane. By careful statistical analysis, additional features are obtained.

First, the intrinsic fluctuations are obtained by smoothing the maps with a Gaussian of 7° FWHM, which when convolved with the 7° FWHM antenna beam, results in about a 10° smoothing on the sky. The intrinsic sky temperature fluctuation σ_{Sky} is 30±5 μK for $|b|>20°$.

The quadrupole anisotropy is shown in all six channels. By separating the Galactic emission,[59] a cosmic signal with a rms-normalized amplitude $Q_{rms}=13\pm4$ μK is found. Here, the quadrupole $Q(l, b)$ is expanded as $Q(l, b)=Q_1(3\sin^2 b-1)/2+Q_2\times\sin 2b\cos l+Q_3\sin 2b\sin l+Q_4\cos^2 b\cos 2l+Q_5\cos^2 b\sin 2l$, and Q_{rms} is defined as $Q_{rms}\equiv(4/15)((3/4)Q_1^2+Q_2^2+Q_3^2+Q_4^2+Q_5^2)$.

COBE group also obtained the temperature correlation function, $C(\theta)=\langle\Delta T_1\Delta T_2\rangle$, which is the average product of temperature fluctuation separated by angle θ with a 3.2° effective Gaussian smoothing.

4.3. *Constraint on the models without the cosmological constant*

As mentioned in § 4.2, *COBE* has detected the quadrupole amplitude of the CMB fluctations and the intrinsic Gaussian temperature fluctuation smoothed on 10° FWHM, $\sigma_{sky}(10°)$.[3] In this section, we search the models in which the expected CMB anisotropies are consistent with the observed ones in the following procedure:[60] We calculate $\sigma_{sky}(10°)$ in various representative cosmological models including ones with open background. Here $\sigma_{sky}(10°)$ is given by $\sigma_{sky}(\theta_{FWHM}=10°)=[C(\theta=0, \theta_s)]^{1/2}$, where $C(\theta, \theta_s)$ is the intrinsic temperature angular correlation convoluted with a Gaussian smoothing angle θ_s and is given by the ordinary method (see Eq. (2·53)). In the observation of *COBE*, the sky maps of temperature are made by smoothing with a total 10° FWHM Gaussian and then θ_s is 4.°25 as seen in Eq. (2·54).

At first, in each cosmological model we normalize the fluctuation according to the scheme that the expected rms temperature anisotropy ($\tilde{\sigma}(10°)\equiv\sigma_{sky}(10°)/T_0$) is equal to the observed one ($\sigma_{sky}(10°)/T_0=1.1\times10^{-5}$). As mentioned in § 2.5, this normalization scheme has a merit because there is no biasing problem.

And then we estimate theoretically the rms quadrupole moment of the anisotropy $\tilde{Q}_{theory}(\equiv Q_{theory}/T_0)$ according to this normalization in each model. Here according to the definition of the quadrupole moment used by *COBE*, the rms quadrupole moment $\tilde{Q}_{theory}$ is given by

$$\tilde{Q}^2_{theory}=\langle Q_{ij}Q^{ij}\rangle=\frac{3}{2}\frac{1}{2\pi^2}\int_0^\infty \tilde{k}^2 d\tilde{k}\,|\theta_{m(2)}(\eta_0)|^2\frac{(\tilde{k}^2-4K)}{(\tilde{k}^2-K)},$$

$$Q^{ij}\equiv\frac{5}{4\sqrt{7.5\pi}}\int d\Omega(\gamma)\Theta_m P^{ij}_{(2)}\,, \tag{4·4}$$

where $\tilde{k}^2\equiv k^2+K$ and the definition of Q_{theory} is the same as that of Q_{rms} by *COBE* shown in § 4.2. We must mind that the definition of the quadrupole moment is different from each other among the authors (see in detail Ref. 69)). Here $\theta_{m(2)}$ is estimated by the method mentioned in § 2.5. Again it must be remarked that the CMB quadrupole moment, of course, has been calculated by many authors.[9)~11),61)~68)] However, all of these were unsatisfactory in the sense that their considerations were restricted either to the spatially flat background or to an incomplete evaluation of the quadrupole moment. In other words, so far there has appeared no work which considers an open universe model and completely includes both the generalized Sachs-Wolfe effect[10)] or Rees-Sciama effect and intrinsic photon fluctuations at decoupling in evaluating the quadrupole moment. This unsatisfactory situation is mainly due to a technical difficulty in estimating the present quadrupole and/or higher multipoles of the CMB anisotropy in an open universe. However, we have succeeded in deriving a formula by which one may calculate any multipole moment of the CMB anisotropy with practically arbitrary precision as shown in § 2.5.

Finally, we compare the expected quadrupole moment $\tilde{Q}_{theory}$ in each model with the observed one ($Q_{rms}/T_0=5\times10^{-6}$) and search the models whose quadrupole moment is consistent with the observed one. In this comparison, we must note that the *theoretically* expected rms quadrupole moment is not directly comparable to the observed one and the quadrupole moment in our universe will be distributed like χ^2 with 5 degrees of freedom under the assumption of random phase Gaussian distribution.[70)] Hence it follows that there is a probability of 90 % of measuring a rms quadrupole $\tilde{Q}_{rms}$.

$$0.48<\frac{\tilde{Q}_{rms}}{\tilde{Q}_{theory}}<1.5\,.$$

Moreover we estimate the temperature anisotropy $\delta T/T$ at 7.′15 and at 1° in each model using the temperature fluctuations normalized according to the above scheme. Comparing the results with the observed upper limits of $\delta T/T$ at 7.′15 by Readhead et al.[25)] and at 1° by Meinhold and Lubin,[27)] we constrain models more severely than from only the large-angular anisotropy alone.

Furthermore we consider whether or not the matter fluctuations in the allowed models are consistent with the observed quantities of matter structures such as galaxy two-point correlation functions and so on. Here we try to constrain the models by examining whether the expected $J_3(25h^{-1}\,\mathrm{Mpc})$ in each model is consistent with the observed value, $780\,\mathrm{Mpc}^3h^{-3}$. We estimate the biasing factor b in each model, which is defined by $b\equiv\sqrt{C(0,10^\circ,J_3)/C(0,10^\circ,COBE)}$, where $C(0,10^\circ,J_3)$ is the intrinsic temperature angular correlation function estimated according to the normalization scheme by $J_3(25\,h^{-1}\,\mathrm{Mpc})$ and $C(0,10^\circ,COBE)$ is the observed one by *COBE*. We assume from the definition of b that the allowed models for the constraints by anisotropies of the CMB in Table I are still survived if $b\lesssim5$.

The models that we have examined are baryon-dominated universe models

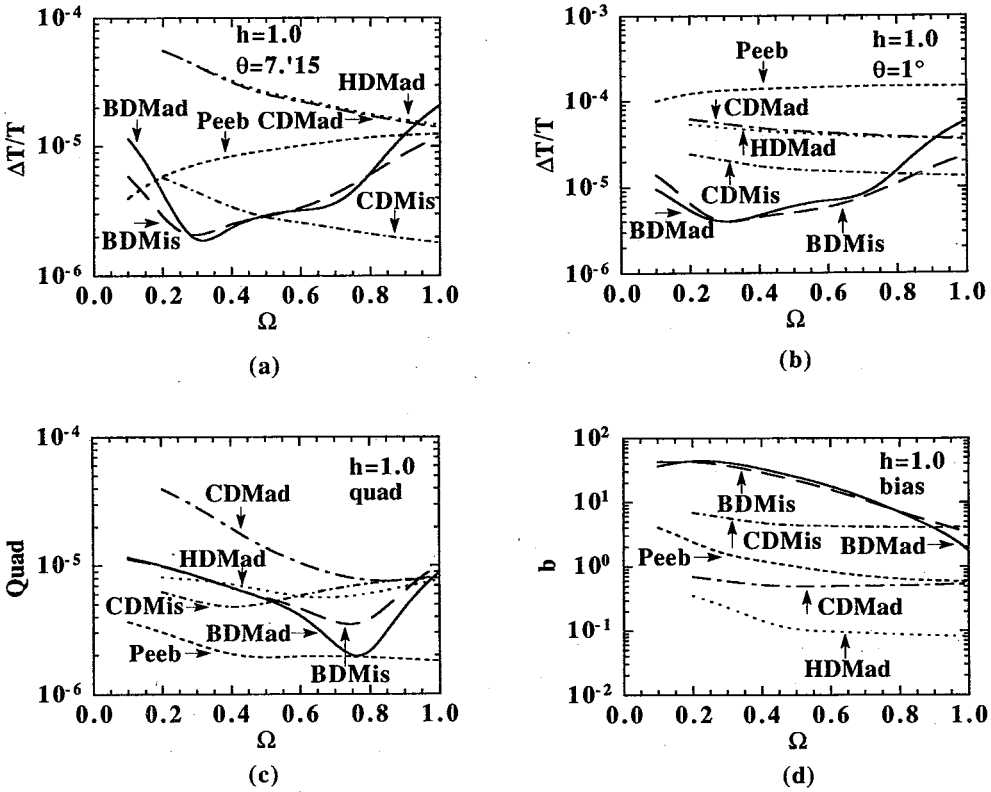

Fig. 15.(a) The predicted anisotropies of the CMB at 7.'15 for various models with $h=1.0$ as a function of Ω_0. The models shown here are adiabatic BDMs(BDMad), isocurvature BDMs(BDMis), Peebles' model(Peeb), adiabatic CDMs(CDMad), isocurvature CDMs(CDMis) and adiabatic HDMs (HDMad). The initial power-law index n in the models shown here is 1 though only in Peebles' model n is 3. In these models the cosmological constant vanishes.

(b) The predicted anisotropies of the CMB at 1° for various models with $h=1.0$ as a function of Ω_0. The models shown here are the same as shown in (a).

(c) The predicted quadrupole moments of the CMB anisotropies for various models with $h=1.0$ as a function of Ω_0. The models shown here are the same as shown in (a).

(d) The predicted biasing parameters, b, for various models with $h=1.0$ as a function of Ω_0. The models shown here are the same as shown in (a).

(BDMs); cold dark matter models(CDMs) with initially adiabatic and axionic isocurvature perturbations; hot dark matter models(HDMs) with initially adiabatic perturbation; and Peebles' reionized universe models.[12),37)] As for dark matter dominated models, we set the baryon density parameter $\Omega_b=0.03$. We have taken the non-dimensional Hubble parameter h normalized by 100 km/s/Mpc, 0.5 and 1.0. Models with initial power spectrum $n=0, 1$ and 2 have been calculated except Peebles' models. As for Peebles' models, higher initial power is needed to reionize the interstellar matter and we have chosen $n=1, 2$ and 3. Here, we have neglected the secondary effect on CMB fluctuations induced by ionized matter, so-called Vishiniac effect[50),51)] for Peebles' models. This effect plays an important role on small scale fluctuations, but do not produce large scale anisotropies. In our calculations, neglecting this effect may make the expected fluctuations on 7.'15 scale underestimated. As

Table I. Constraints on Cosmological Models without Cosmological Constant

model			7.15 min.	1 deg.	Quadrupole	bias	All
BDM adiabatic	$h=1.0$	$n=0$	No Constraint	No Constraint	$0.52<\Omega<0.93$	No Region	No Region
		$n=1$	No Constraint	$\Omega<0.92$	$0.21<\Omega$	$0.85<\Omega$	$0.85<\Omega<0.92$
		$n=2$	$0.37<\Omega<0.43$	$0.12<\Omega<0.52$	$\Omega<0.56$ $0.90<\Omega$	$0.41<\Omega$	$0.41<\Omega<0.43$
	$h=0.5$	$n=0$	No Constraint	No Constraint	$0.35<\Omega<0.92$	No Region	No Region
		$n=1$	$0.18<\Omega$	$\Omega<1.0$	$\Omega<0.55$ $0.84<\Omega$	$0.86<\Omega$	$0.86<\Omega<1.0$
		$n=2$	No Region	No Region	$\Omega<0.45$ $0.89<\Omega$		No Region
BDM isocurvature	$h=1.0$	$n=0$	No Constraint	No Constraint	$0.55<\Omega<0.89$	No Region	No Region
		$n=1$	No Constraint	No Constraint	$0.21<\Omega$	$0.89<\Omega$	$0.89<\Omega$
		$n=2$	No Region	$0.14<\Omega<0.63$	$\Omega<0.57$ $0.84<\Omega$	$0.31<\Omega$	No Region
	$h=0.5$	$n=0$	No Constraint	No Constraint	$0.29<\Omega<0.80$	No Region	No Region
		$n=1$	No Constraint	$0.13<\Omega$	$\Omega<0.95$	No Region	No Region
		$n=2$	No Region	No Region	No Constraint		No Region
Peebles	$h=1.0$	$n=1$	No Constraint	No Constraint	$\Omega<0.93$	No Region	No Region
		$n=2$	No Constraint	No Region	No Constraint	$0.28<\Omega$	No Region
		$n=3$	No Constraint	No Region	$\Omega<0.18$		No Region
	$h=0.5$	$n=1$	No Constraint	No Constraint	$\Omega<0.88$	No Region	No Region
		$n=2$	No Constraint	$\Omega<0.20$	No Constraint	$0.56<\Omega$	No Region
		$n=3$	No Constraint	No Region	$\Omega<0.45$		No Region
CDM adiabatic	$h=1.0$	$n=0$	No Constraint	No Constraint	No Region	$0.27<\Omega$	No Region
		$n=1$	$0.65<\Omega$	$\Omega\sim1.0$	$0.62<\Omega$		$\Omega\sim1.0$
		$n=2$	No Region	No Region	$0.53<\Omega$		No Region
	$h=0.5$	$n=0$	No Constraint	No Constraint	No Region	No Region	No Region
		$n=1$	$0.76<\Omega$	$0.87<\Omega$	$0.67<\Omega$		$0.87<\Omega$
		$n=2$	No Region	No Region	$0.59<\Omega$		No Region
CDM isocurvature	$h=1.0$	$n=0$	No Constraint	No Constraint	$\Omega<0.54$	No Region	No Region
		$n=1$	No Constraint	No Constraint	No Constraint	$0.37<\Omega$	$0.37<\Omega$
		$n=2$	$0.55<\Omega$	No Region	No Constraint		No Region
	$h=0.5$	$n=0$	No Constraint	No Constraint	$\Omega<0.55$	No Region	No Region
		$n=1$	No Constraint	$0.10<\Omega$	No Constraint	No Region	No Region
		$n=2$	$0.40<\Omega$	No Region	No Constraint		No Region
HDM adiabatic	$h=1.0$	$n=0$	No Constraint	No Constraint	$0.40<\Omega<0.60$	$0.45<\Omega$	$0.45<\Omega<0.60$
		$n=1$	$0.65<\Omega$	No Region	No Constraint		No Region
		$n=2$	No Region	No Region	$\Omega<0.59$ $0.97<\Omega$		No Region
	$h=0.5$	$n=0$	No Constraint	No Constraint	No Region	No Region	No Region
		$n=1$	$0.78<\Omega$	$0.72<\Omega$	No Constraint	$0.21<\Omega$	$0.78<\Omega$
		$n=2$	No Region	No Region	$\Omega<0.68$		No Region

Note: If there remains no allowed region on the density parameter, we indicate No Region. If the model is not constrained, we indicate No Constraint. As for bias parameter b, constraints are obtained from the condition that b must be less than 5. So empty means $b<5$ through all region of Ω.

a result, the constraint on Peebles' models by the small scale observation may be slightly more strict than those obtained in this paper.

Here it must be noticed that Wright et al.[71] also analyzed some cosmological models using the results of *COBE*, however, there are some differences from ours. Please refer to Ref. 60) on the detailed explanations of these differences.

In Figs. 15(a)~(d), the predicted anisotropies of the CMB at 7.15, 1° quadrupolemoments and biasing parameters in various models with $n=1$ are shown, respectively.

Constraints are obtained at 90 % confidence level as previously mentioned. Including the constraints by the small scale anisotropies and the biasing parameter, results for all models are shown in Table I.

First, we show the constraints obtained by only using the observations of the CMB anisotropies, that is, the observed quadrupole moment by *COBE* and the upper limit of $\delta T/T$ at 7.'15 by Readhead et al.[25] and 1° by Meinhold and Lubin.[27] We found from Table I that models with $n>1$ are constrained mainly from the result by Readhead et al. and models with $n\sim1$ and $n<1$ are restricted mainly from the observations by Meinhold and Lubin and *COBE*, respectively. If we consider models which are consistent with the inflationary scenario such that $\Omega_0=1$ and $n=1$, BDMs with initially adiabatic perturbations and $h=0.5$, isocurvature BDMs with $h=1.0$, HDMs with $h=0.5$, CDMs with adiabatic perturbations and $h=0.5$ and isocurvature CDMs are survived and both adiabatic CDMs and adiabatic HDMs with $h=1.0$ are marginally alive. On the other hand, if we believe the dynamical estimates on the density parameter, i.e., $0.1<\Omega_0<0.3$ (see, e.g., Ref. 37)), all BDMs with $n=1$, Peebles' reionized universe models with $n=1$ or isocurvature CDMs with $n<2$ can explain such low value of Ω_0. It should be noted that we neglect the observational error when constraints on cosmological models are set. Including the observational error, however, constraints obtained here by the quadrupole anisotropy are still 80 % confidence level.

As shown above, there are relatively many allowed models for the constraints by the CMB anisotropies. Next we consider whether the allowed models for the constraints by the CMB anisotropies are consistent with the assumption that $b\lesssim5$. The result is as follows: Adiabatic BDMs, isocurvature BDMs with $\Omega_0\sim1.0$ and $n=1$ and adiabatic BDM with $\Omega_0\sim0.4$ and $n=2$ might be marginally allowed since $b\sim4$. However it might be difficult to expect that $b\gg1$ for BDMs and moreover we cannot expect such large baryon densities from the primordial nucleosynthesis.[72] Although the reionized universe scenario is considered, it is difficult to save isocurvature baryon dominated universe since Peebles' models with $n=1$ must be large biasing factor $b\gtrsim10$. Moreover it is difficult for models with scale invariant initial spectrum $n=1$ to produce ionized matter since reheating of the universe may be caused by higher power spectrum. The biasing parameter of adiabatic CDMs and HDMs with $n=1$ and both $h=1.0$ and $h=0.5$ is nearly equal to less than 1 and these models with $\Omega_0\simeq1$ are desirable. Moreover adiabatic HDMs with $0.45<\Omega_0<0.60$, $h=1.0$ and $n=1$ is alive. As for isocurvature CDMs, there is still surviving model with $\Omega_0>0.37$, $h=1.0$ and $n=1$. The allowed models for all the constraints are shown in Table I.

Basically, the normalization scheme based on other observed quantities, e.g., J_3 at other scales, correlation function itself and peculiar velocities yields the similar amplitudes of the fluctuations within the factor 2 or so over a wide range of parameters.[19),20] Then we will get the similar results shown above when estimating the constraint on the model from other quantities of matter structures and/or peculiar velocities.

As a result, if the cosmological constant vanishes, only dark matter dominated models with $n\simeq1$ and $\Omega_0\simeq1$ are desirable while there is a possibility that the universe has low density for isocurvature CDMs and adiabatic HDMs.

4.4. *Constraint on the models with the cosmological constant*

Following the same strategy in § 4.3, we search the cosmological models with the

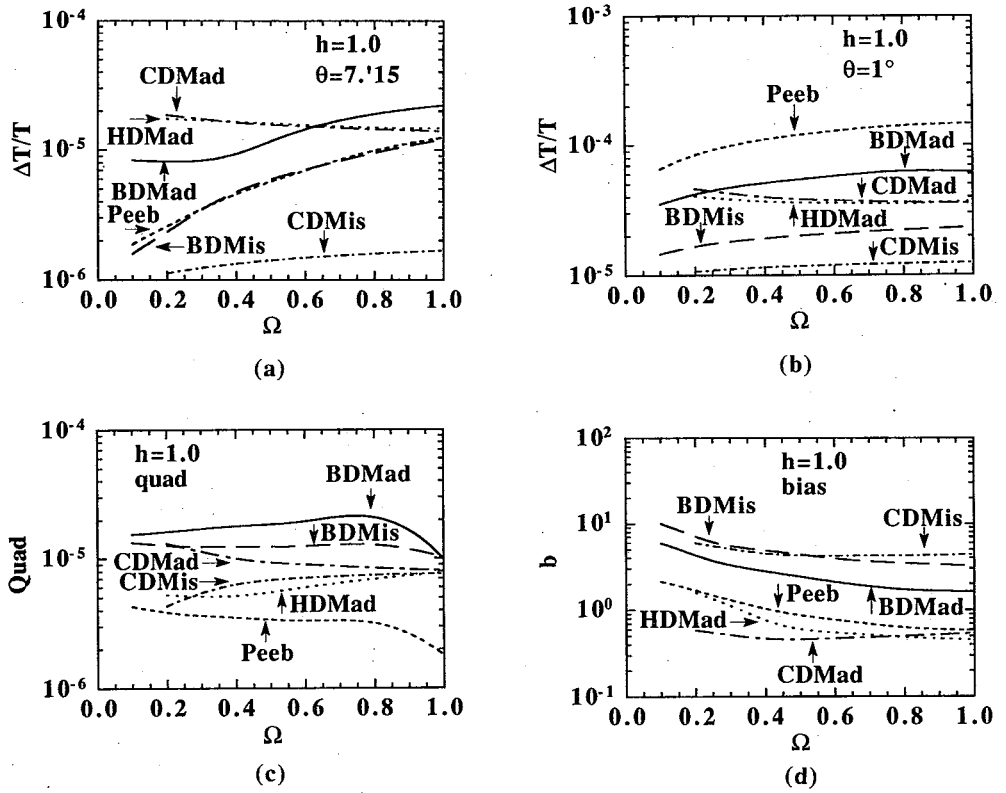

Fig. 16.(a) The same as Fig. 15(a), but for the models with the cosmological constant.
(b) The same as Fig. 15(b), but for the models with the cosmological constant.
(c) The same as Fig. 15(c), but for the models with the cosmological constant.
(d) The same as Fig. 15(d), but for the models with the cosmological constant.

cosmological constant which are consistent with the observations. Here we consider only the models with totally flat geometry, i.e., $\Omega_0+\lambda=1.0$.

We show the predicted temperature fluctuations at 7.'15, 1° and quadrupole-moments and biasing parameters in various models with the cosmological constant and $n=1$ in Figs. 16(a)~(d), respectively.

The results are summarized in Table II. At first, we show the constraints only by the CMB anisotropies. We found in this case that there are more allowed models than in the case without the cosmological constant for the restriction especially on the small angle scale. This reason is explained in § 3.5. As for BDMs, almost all models are excluded except for isocurvature BDMs with $\Omega_0=h=1.0$ and $n=1.0$. But BDMs with $\Omega_0=\Omega_b\sim1.0$ is prohibited from the primordial nucleosynthesis. There are still allowed cases for Peebles' models with low Ω_0. As for CDMs and HDMs, there are wider allowed ranges of the cosmic parameters than those for the models without the cosmological constant. As for Peebles' models with $h=0.5$, $n=3$ and HDMs with $h=1.0$ and $n=1.0$, we might say that there are marginally allowed regions, i.e., $\Omega_0\lesssim0.1$ and $0.5<\Omega_0<1.0$, respectively, since $\delta T/T\sim3.5\times10^{-5}$ on 1° in these models though we remarked "No Region" in Table II.

Furthermore we examine the biasing factor b in the allowed models for the constraints by the CMB anisotropies. We assume that models with $b\lesssim5$ are still

Table II. Constraints on Cosmological Models with Cosmological Constant

model			7.15 min.	1 deg.	Quadrupole	bias	All
BDM adiabatic	$h=1.0$	$n=0$	No Constraint	No Constraint	No Region	No Region	No Region
		$n=1$	No Constraint	$\Omega<0.10$	$\Omega\sim1.0$	$0.15<\Omega$	No Region
		$n=2$	No Region	No Region	$0.90<\Omega$		No Region
	$h=0.5$	$n=0$	No Constraint	No Constraint	No Region	No Region	No Region
		$n=1$	No Constraint	$\Omega<0.63$	$\Omega\sim1.0$	$0.51<\Omega$	No Region
		$n=2$	No Region	No Region	$0.91<\Omega$		No Region
BDM isocurvature	$h=1.0$	$n=0$	No Constraint	No Constraint	No Region	No Region	No Region
		$n=1$	No Constraint	No Constraint	$\Omega\sim1.0$	$0.37<\Omega$	$\Omega\sim1.0$
		$n=2$	$\Omega<0.31$	No Region	No Constraint		No Region
	$h=0.5$	$n=0$	No Constraint	No Constraint	No Region	No Region	No Region
		$n=1$	No Constraint	No Constraint	No Region	No Region	No Region
		$n=2$	$\Omega<0.90$	No Region	No Constraint		No Region
Peebles	$h=1.0$	$n=1$	No Constraint	No Constraint	$\Omega\sim1.0$	No Region	No Region
		$n=2$	No Constraint	$\Omega<0.12$	No Constraint	$0.18<\Omega$	No Region
		$n=3$	No Constraint	No Region	$\Omega<0.80$		No Region
	$h=0.5$	$n=1$	No Constraint	No Constraint	$\Omega<0.88$	No Region	No Region
		$n=2$	No Constraint	$\Omega<0.47$	$0.42<\Omega$	$0.48<\Omega$	No Region
		$n=3$	No Constraint	No Region	$\Omega<0.95$		No Region
CDM adiabatic	$h=1.0$	$n=0$	No Constraint	No Constraint	No Region		No Region
		$n=1$	No Constraint	$\Omega\sim1.0$	$0.44<\Omega$		$\Omega\sim1.0$
		$n=2$	No Region	No Region	$0.32<\Omega$		No Region
	$h=0.5$	$n=0$	No Constraint	No Constraint	No Region	No Region	No Region
		$n=1$	No Constraint	$0.70<\Omega$	$0.26<\Omega$		$0.70<\Omega$
		$n=2$	No Region	No Region	$0.20<\Omega$		No Region
CDM isocurvature	$h=1.0$	$n=0$	No Constraint	No Constraint	$\Omega<0.33$	No Region	No Region
		$n=1$	No Constraint	No Constraint	No Constraint	$0.30<\Omega$	$0.30<\Omega$
		$n=2$	No Constraint	No Region	$0.27<\Omega$		No Region
	$h=0.5$	$n=0$	No Constraint	No Constraint	$\Omega<0.33$	No Region	No Region
		$n=1$	No Constraint	No Constraint	No Constraint	No Region	No Region
		$n=2$	No Constraint	$0.45<\Omega$	$0.29<\Omega$		$0.29<\Omega<0.45$
HDM adiabatic	$h=1.0$	$n=0$	No Constraint	No Constraint	$\Omega<0.43$	$0.38<\Omega$	$0.38<\Omega<0.43$
		$n=1$	No Constraint	No Region	No Constraint		No Region
		$n=2$	No Region	No Region	$0.95<\Omega$		No Region
	$h=0.5$	$n=0$	No Constraint	No Constraint	$\Omega<0.39$	No Region	No Region
		$n=1$	No Constraint	$0.60<\Omega$	No Constraint		$0.60<\Omega$
		$n=2$	No Region	No Region	No Region		No Region

Note: The same as Table II but the constraints on models with $\lambda+\Omega=1$ are shown.

alive. As a result, we conclude that all BDMs with low density are excluded even if they have the cosmological constant. Peebles' models with $\Omega\lesssim0.1$, $h=0.5$ and $n=3$ might be marginally allowed even when we consider the constraint by the biasing parameter, while we remarked "No Region" in Table II. As for adiabatic CDMs, the allowed regions of the cosmic parameters are $\Omega_0\sim1.0$, $h=1.0$ and $n=1$ and $\Omega_0>0.7$, $h=0.5$ and $n=1$. As for isocurvature CDMs, they are $\Omega_0>0.3$, $h=1.0$ and $n=1$ and $0.29<\Omega_0<0.45$, $h=0.5$ and $n=2$. Adiabatic HDMs with $\Omega_0>0.6$, $h=0.5$, $n=1$ and HDMs with $0.38<\Omega_0<0.43$, $h=1.0$, $n=0$ are still alive. Moreover adiabatic HDMs with $0.5<\Omega_0<1.0$, $h=1.0$ and $n=1$ are marginally allowed while we remarked "No region" in Table II.

Here it must be noticed that the theoretical estimation of the angular correlation function $C(\theta)$ goes to infinity if we consider the density fluctuations with $k\to0$ and n

≤ 1 in the flat universe as seen Eq. (2·55). Although the density fluctuations on super-horizon scales might be created at the epoch of the inflationary universe, we think that they might be neglected since we can now contact the fluctuations causally only within the present horizon scale. Then we cut off the integration in Eq. (2·55) at the wavenumber corresponding to the present horizon scale. However the convergence of the integration is not well, so we have to mind the range of the wavenumber for the integration. We treated carefully this integration for all models both without and with the cosmological constant in this analysis and then the quantitative estimation of the models without the cosmological constant are slightly changed compared with the estimation in the previous our work[60] while the final results are not so much changed.

4.5. *Topology of cosmic background fluctuations*

We have constrained the galaxy models in which density fluctuations are assumed implicitly to grow from the initially Gaussian fluctuation due to the gravitational instability. The temperature fluctuations which have been estimated in the models give the dispersion of the fluctuations and the observational results which have given by using the χ^2 test also give the dispersion. Provided that the present temperature fluctuations obey the Gaussian statistics, the comparison of the values of temperature fluctuations in theory with the observed ones are meaningful. However there might be a possibility that the initial fluctuations are non-Gaussian fluctuations and/or the density fluctuations grow due to the non-linear effect (e.g., cosmic strings or domain walls) beside the instability of the self-gravity. In these cases, the present temperature fluctuations might obey the non-Gaussian statistics. Then the comparison of the dispersions of the temperature fluctuations given in theory with ones of the observations might not be meaningful. In this case, however, a good method is proposed of comparing the theories and the observations. This is the topological measure; the total curvature (genus) of the isotemperature contours are often used to study for the maps of the cosmic microwave fluctuations.[73] By using the relation of the genus to the threshold of the isotemperature contour, statistical properties such as Gaussian behavior and the power spectrum of the temperature field are analyzed analytically. Then we can easily determine whether the temperature fluctuations are Gaussian or not. This method is also applied to the study for the topology of the large-scale structures (see references in Ref. 73)). In the near future, *COBE* will show the temperature gradient map with more precision. Then the topological measure, such as genus will be useful to study the simulated microwave background anisotropy maps in a model and then to compare them with those of the observations.

§ 5. Other effects on CMB anisotropies

We constrained the galaxy formation models from both small-angle scales and quadrupole moment of CMB anisotropies. However some phenomena which we do not consider in the above estimation of the present temperature fluctuations would influence the small-angle scale anisotropies of the CMB. Among these effects, we comment about the effect of gravitational lens, the non-linear effect of the growth of

matter density fluctuations and the effect on the CMB by the hot plasma of the intergalactic medium. It should be noted that the large-angle anisotropies of CMB would not be influenced by such local effects.

5.1. *Effect of the gravitational lens*

It had been pointed out that CMB anisotropies on small angular scales might be strongly suppressed due to the gravitational lens effect during the propagation of the radiation from the last scattering surface to the present time. Hence the constraint on the galaxy models is supposed to be weakened by this gravitational lens effect.[74] However Sasaki[75] has pointed out clearly that the anisotropies on scales smaller than a characteristic coherence angle associated with the lens distribution may be enhanced, while those on larger scales are suppressed as usually expected if the characteristic angular scale associated with the gravitational lens effect is comparable to the coherence angle of the cosmic microwave anisotropy. That is, the gravitational lensing may enhance anisotropies at $\theta \lesssim \theta_c$ if $\theta_g \gtrsim \theta_D \sim \theta_c$, where θ_c is the intrinsic coherence angle of the CMB anisotropy, θ_g is the characteristic deflection angle by gravitational lensing, and θ_D is the characteristic angle determined by the coherence length of gravitational potential inhomogeneities (see the detailed definitions of the angle scales in Ref. 75)).

However we have to take into account the finite beam width, σ, of a telescope when we relate the gravitational lens effect to an observation and the effect of enhancement or suppression depends on the angular sizes of σ, θ_c, θ_g and θ_D while the result mentioned above remain true if σ is appreciably smaller than θ_c. These angle sizes depend on the models and the experiments. Then we have to take into account the gravitational effect in each model when estimating the small angular anisotropies in the model and comparing them with the results of observations, while a few models have been analyzed and it is found that the anisotropies of the CMB would be decreased by a few decade percent in the models.[76]

5.2. *Effect of the non-linear growth of density fluctuations*

We estimated the density fluctuations in the linear analysis. However matter density fluctuations grow into the non-linear stage and then the linear analysis breaks out. The non-linearity of the growth of matter density fluctuations may reflect the estimation of the temperature fluctuations as follows.

(1) We estimated J_3 by using the present matter density perturbations which are analyzed in the linear analysis when we constrain the models. Then the estimated J_3 may be changed when we estimated the present matter density fluctuations in taking into account the non-linear growth. And so constraint on the models will be changed while the results in the linear analysis will not change so appreciably when using the J_3 on very large-scales.

(2) The present photon fluctuation is described by Eq. (2·44). θ_{dif} vanishes for flat universe models because the gravitational potential perturbation does not change with time increasing in the linear analysis. As for open universe models the potential perturbations change especially the later stage even in the linear analysis. However

θ_{dif} does not contribute dominantly to the total photon fluctuations on small angular scales while it contribute dominantly to the quadrupole moment of CMB anisotropies as shown in Gouda et al.[15] The non-linear growth of density perturbations, of course, reflect the time evolution of the potential perturbations and may change the estimation of θ_{dif} even in the flat universe. We must consider this effect in estimating the CMB anisotropies on both small-angular scales and large-angle scales while some works have been done for the special models[77),78)] and it is found that the non-linear effect of very large scale structures would create temperature fluctuations by the amount of a few times 10^{-6} and more larger ones.

5.3. *Secondary temperature fluctuations induced by hot gas*

Usually, it is assumed that recombination occurs at the time of $z\sim1000$ and that the intergalactic medium remains neutral thereafter. In that case, perturbations of photon are freely streaming from the last sccattering surface to us and do not change their rms amplitude, as shown in § 2. Under some special situations such that the intergalactic medium is reionized, however, it happens that new fluctuations are produced. Here, we briefly review these secondary temperature fluctuations.

(a) Sunyaev-Zeldovich effect[79)]

In the hot ionized medium, distortion of the black body spectrum of the CMB occurred as a result of inverse Compton scattering from thermal electrons. This is known as Sunyaev-Zeldovich effect. The Kampaneetz equation which describes the evolution of the photon distribution function due to repeated, nonrelativistic inverse Compton scattering is

$$\frac{\partial n}{\partial t_c}=\frac{kT_e}{m_ec^2}\frac{1}{x^2}\frac{\partial}{\partial x}\left[x^4\left(\frac{\partial n}{\partial x}+n+n^2\right)\right], \tag{5·1}$$

where n is the occupation number of photon $t_c\equiv(n_e\sigma_Tc)t$, T_e and m_e are electron temperature and elecron mass and $x\equiv h\nu/kT$ with n_e, σ_T, ν and T being the electron number density, the Thomson cross-section, the radiation frequency and radiation temperature, respectively. Here, the speed of light is shown in equations because of the clearness of the physical meaning for quantities. Following Kampaneetz, the dimensionless variable, Compton y parameter is introduced as

$$y=-\int_0^\tau\frac{kT_e}{m_ec^2}d\tau\,, \tag{5·2}$$

where $\tau\equiv\int\sigma_Tn_edl$ is the optical depth due to Thomson scattering. The physical meaning of y parameter is the fractional energy change of photon energy by the Compton scattering. In the case $T_e\gg T_r$, the Kampaneetz equation is rewritten as

$$\frac{\partial n}{\partial y}=\frac{1}{x^2}\frac{\partial}{\partial x}x^4\frac{\partial n}{\partial x}\,. \tag{5·3}$$

This equation can be easily solved for small values of y when the deviations from a Planck spectrum are small. By inserting in the right-hand side the unperturbed Planck function $n_0(x)=1/(e^x-1)$, we obtain

$$\frac{\Delta n}{n_0}=\frac{\Delta J}{J_0}=\frac{e^x}{e^x-1}xy\left(\frac{x}{\tanh(x/2)}-4\right), \tag{5·4}$$

where $J=(2h\nu^3/c^2)n$ is the specific intensity or brightness. Then, the temperature fluctuation is obtained as

$$\frac{\Delta T}{T_0}=\frac{\Delta J}{J_0}/\frac{d\ln J}{d\ln T}=y\left(\frac{x}{\tanh(x/2)}-4\right). \tag{5·5}$$

Taking the limit of small x, i.e., $h\nu/kT\ll 1$, the expected temperature fluctuation is obtained as $\Delta T/T_0=-2y$ or

$$T=T_0e^{-2y}. \tag{5·6}$$

In clusters of galaxies, the temperature decrease towards the center has been detected indeed.[80)~82)] From the observations of Sunyaev-Zeldovich effect, we can directly obtain the information of intergalactic medium. And combining the observations of Sunyaev-Zeldovich effect with the observations by the X-ray we can know the distance to the clusters of galaxies.[83)] In the near feature, the value of the Hubble constant will be determined by this method.

We have believed that the Sunyaev-Zeldovich effect affects the CMB only on a small scale less than one arcminute. However Makino and Suto[84)] show this effect also plays an important role on arcminutes scale. We may have to take into account this effect when we examine the cosmological models by the observational results on a few arcminutes.

b) Velocity induced fluctuations[51),50)]

If the reheating occurs in the whole universe after the decoupling of baryon-photon, the primary anisotropies of CMB generated before the decoupling are modified. The Peebles' model that the universe remains fully ionized until the present is the extreme example. In such reionized universe, the Plank function f obeys not a collisionless (Eq. (2·40)) but a collisional Boltzmann equation. The gauge invariant form of the radiative transfer is[22)]

$$\Theta_s'+\gamma^i\partial_i\Theta_s=-(\Phi'+\gamma^i\partial_i\Psi)+an_e\sigma_T\left[\frac{1}{4}\Delta_{sr}-\Theta_s-\gamma^i\partial_iV_b+\frac{1}{6}\Pi_{ij}\gamma^i\gamma^j\right], \tag{5·7}$$

where $'$ denotes the derivative according to conformal time, Δ_{sr} is the photon density perturbation on the shear free hypersurface and the suffix b denotes baryon. Other notations are shown in § 2. The relation between Δ_{cr} and Δ_{cs} is $\Delta_{cr}=\Delta_{sr}+4(a'/a)V/k$. Even after *last scattering* at the time when the optical depth from the present epoch equals unity, the collisional term on the right-hand side of the above equation produces secondary temperature fluctuations. Roughly speaking, fluctuations are induced by the electron bulk velocity. It is very interesting that the first order anisotropies are not so efficient in temperature fluctuations because the different phases of any single plane wave will cancel out each other.[50)] Hence the second order contributions led by fluctuations in electron density n_e become efficient on the small angle scale. This is known as Vishiniac effect.

As for Peebles' models, in particular, these secondary velocity induced fluctua-

tions are comparable with or sometimes exceed the primary ones which we calculated. As results of numerical calculations,[85] the second order term of velocity induced fluctuations is dominated on a few arcminutes angle scale. On a few tens arcminutes angle scale, the primary terms, first order and second order components of secondary terms give approximately the same contributions on the observed temperature anisotropies. The temperature anisotropies of the scale larger than a degree, the primary term is dominated.

§ 6. Conclusions and discussion

The anisotropies of the CMB give very important information about the formations of the large-scale structures of the universe. For a long time, the intrinsic CMB anisotropies had not been detected. At last, however, *COBE* has discovered the large-angle anisotropies of the CMB. By using the results of *COBE*, we can constrain the cosmological models for formations of the large-scale structures more severely and strictly than before. However, in fact, as shown in §§4.3 and 4.4, there are still many surviving models by using only *COBE*'s results as shown in Tables I and II. But when we consider whether these allowed models are consistent with the upper limits of the small-angle anisotropies of the CMB and/or the observed J_3, we found that the desirable models without the cosmological constant are dark matter dominated models with $n\simeq 1$ and $\Omega_0=1$ while there is still a possibility that the universe has low density for isocurvature CDMs and adiabatic HDMs. It is remarkable that these models are just consistent with inflationary scenario. The angular resolution of *COBE*'s data is 7° which is larger than the horizon scale at the recombination. Then the fluctuations observed by *COBE* are completely uncausal at the recombination epoch. Since only the inflation can make uncausal regions which is once casually connected,[86] it may be the proof of the inflationary scenario that such fluctuations exist.

As for the models with the cosmological constant, there are wider allowed regions of the cosmic parameters, Ω_0, h and n. Although BDMs even with the cosmological constant are excluded, Peebles' models with $\Omega_0\lesssim 0.1$, $h=0.5$ and $n=3$ might be marginally allowed. As for dark matter models, the allowed regions of the parameters are extended wider than those for the models without the cosmological constant. That is, the models with lower Ω_0 are still survived if the cosmological constant exists and moreover they are still consistent with the inflationary scenario if they are totally flat universe, that is, $\Omega_0+\lambda=1.0$.

Recently Gould[87] claimed that the *local* value of Q_{rms} estimated by *COBE* group[3] is not correct because of the large errors. He proposed that it is better in this case to estimate the *cosmological* Q_{rms} and he suggested that the *cosmological* Q_{rms} is 8^{+16}_{-8} μK for 90 % confidence level. The *cosmological* Q_{rms} is the value which can be compared directly to the theoretically estimated Q_{theory} in our analysis. Following this suggestion, the models which have $0.0<\tilde{Q}_{theory}=Q_{theory}/T_0<8.8\times 10^{-6}$ are consistent with the observation for 90 % confidence level. In this procedure, as for the restriction from the quadrupole moment the allowed regions are extended for the case $n=2$. However we found that almost final results shown before are not changed.

As stated in § 4.5, provided that the present temperature fluctuations do not obey the Gaussian statistics, it is not a good method to consider only the dispersions of temperature fluctuations in theory and observations. *COBE* will show the temperture map of the CMB with more precision, then we will be able to determine whether the intrinsic fluctuations are Gaussian or non-Gaussian by analyzing the topology of the map, for example, the genus of the isotemperature contours.

Furthermore we can expect the small angle scale anisotropies of the CMB will be detected in the near future. But the theoretical estimation of the small-angular scale anisotropies might be changed if we consider the local effect which might influence the estimation of the CMB anisotropies. We have not examined in detail yet, such as the gravitational lens effect and the effect of reionization after the decoupling era though these local effects would not reflect the large-angular anisotropies of the CMB($>1^\circ$). Then we have to investigate these effects in datail for any model.

Moreover we will get more useful information about the large-scale structures of the universe in the near future beside the further results with more precision by *COBE*. Using the results of these observations, we will be able to get the "*true*" cosmological model in the near future.

Acknowledgements

We would like to thank H. Sato and K. Sato for continuous encouragement. We also thank M. Sasaki for stimulating discussions and useful comments. This work was supported in part by the Grant-in-Aid for Scientific Research Fund from the Ministry of Education, Science and Culture of Japan, No. 04740208.

References

1) A. A. Penzias and R. W. Wilkinson, Astrophys. J. **142** (1965), 419.
2) J. C. Mather et al., Astrophys. J. Lett. **354** (1990), L37.
3) G. F. Smoot et al., Astrophys. J. Lett. **396** (1992), L1.
4) M. J. Geller and J. P. Huchra, Science **246** (1989), 897.
5) A. Dressler et al., Astrophys. J. Lett. **313** (1987), L37.
6) R. K. Sachs and A. M. Wolfe, Astrophys. J. **147** (1967), 73.
7) E. M. Lifshitz, J. Phys. USSR **10** (1946), 116.
8) P. J. E. Peebles and J. T. Yu, Astrophys. J. **162** (1970), 815.
9) M. L. Wilson and J. Silk, Astrophys. J. **243** (1981), 14.
10) M. L. Wilson, Astrophys. J. **273** (1983), 2.
11) N. Gouda and M. Sasaki, Prog. Theor. Phys. **76** (1986), 1016.
12) P. J. E. Peebles, Astrophys. J. Lett. **315** (1987), L73.
13) J. M. Bardeen, Phys. Rev. **D22** (1980), 1882.
14) H. Kodama and M. Sasaki, Prog. Theor. Phys. Suppl. No. 78 (1984), 1.
15) N. Gouda, N. Sugiyama and M. Sasaki, Prog. Theor. Phys. **85** (1991), 1023.
16) S. Weinberg, *Gravitation and Cosmology* (New York, Wiley, 1972).
17) P. J. E. Peebles, *The Large Scale Structure of the Universe* (Princeton University Press, 1980).
18) N. Gouda, M. Sasaki and Y. Suto, Astrophys. J. Lett. **321** (1987), L1.
19) N. Gouda, M. Sasaki and Y. Suto, Astrophys. J. **341** (1989), 557.
20) N. Sugiyama, Prog. Theor. Phys. **81** (1989), 1021.
21) J. R. Bond and A. S. Szaley, Astrophys. J. **276** (1983), 443.
22) H. Kodama and M. Sasaki, Int. J. Mod. Phys. **A1** (1986), 265.
23) J. M. Uson and D. T. Wilkinson, Astrophys. J. Lett. **277** (1984), L1.
24) R. D. Davies et al., Nature **326** (1987), 462.
25) A. C. S. Readhead et al., Astrophys. J. **346** (1989), 566.
26) F. Melchiorri et al., Astrophys. J. Lett. **250** (1981), L1.
27) P. Meinhold and P. Lubin, Astrophys. J. Lett. **306** (1991), L51.

28) S. W. Hawking, Phys. Lett. **115B** (1982), 295.
29) G. Efstathiou and J. R. Bond, Mon. Not. R. Astron. Soc. **227** (1987), 33p.
30) E. J. Groth and P. J. E. Peebles, Astrophys. J. **217** (1977), 385.
31) M. Davis and P. J. E. Peebles, Astrophys. J. **267** (1983), 465.
32) M. Davis et al., Astrophys. J. Lett. **333** (1988), L9.
33) J. Silk, Astrophys. J. **297** (1985), 1.
34) M. Rees, Mod. Not. R. Astron. Soc. **213** (1985), 75p.
35) A. Dekel and M. Rees, Nature **326** (1987), 455.
36) M. Clutton-Brock and P. J. E. Peebles, Astrtophys. J. **86** (1981), 115.
37) P. J. E. Peebles, Nature **327** (1987), 210.
38) N. Vittorio and J. Silk, Astrophys. J. Lett. **297** (1985), L1.
39) R. Juszkiewicz, K. Górski and J. Silk, Astrophys. J. Lett. **323** (1987), L1.
40) Y. Suto, K. Górski, R. Juszkiewicz and J. Silk, Nature **332** (1988), 328.
41) V. C. Rubin et al., Astrophys. J. **81** (1976), 687.
42) C. A. Collins, R. D. Joseph and N. A. Robertson, Nature **320** (1986), 506.
43) A. Dressler et al., Astrophys. J., **313** (1987), 42.
44) N. Kaiser, Mon. Not. R. Astron. Soc. **231** (1988), 149.
45) D. Lynden-Bell et al., Astrophys. J. **326** (1988), 19.
46) S. W. Hawking. Phys. Lett. **115B** (1982), 295.
47) J. Silk, Astrophys. J. **151** (1968), 459.
48) H. Sato, Prog. Theor. Phys. **45** (1971), 370.
49) S. Weinberg, Astrophys. J. **168** (1971), 175.
50) J. P. Ostriker and E. T. Vishniac, Astrophys. J. Lett. **306** (1987), L51.
51) E. T. Vishniac, Astrophys. J. **322** (1987), 597.
52) N. Sugiyama, M. Sasaki and K. Tomita, Astrophys. J. Lett. **338** (1989), L43.
53) N. Sugiyama, N. Gouda and M. Sasaki, Astrophys. J. **365** (1990), 432.
54) F. Occhionero, N. Vittorio, P. Carnevali and P. Santangelo, Astr. Ap. **86** (1980), 212.
55) R. A. Watson et al., Nature **357** (1992), 660.
56) S. S. Meyer, E. S. Chang and L. A. Page, Astrophys. J. Lett. **371** (1991), L4.
57) G. Smoot et al., Astrtophys. J. **360** (1990), 685.
58) G. Smoot, in *Proceedings of Primordial Nucleosynthesis and Evolution of Early Universe* (Kluwer Academic Publishers, 1990), p. 281.
59) C. L. Bennett et al., Astrophys. J. Lett. **396** (1992), L7.
60) N. Gouda and N. Sugiyama, Astrophys. J. Lett. **395** (1992), L59.
61) P. J. E. Peebles, Astrophys. J. **263** (1982), L1.
62) K. Tomita and T. Tanabe, Prog. Theor. Phys. **69** (1983), 828.
63) J. R. Bond and G. Efstathiou, Astrophys. J. Lett. **285** (1984), L45.
64) L. A. Kofman and A. A. Starobinskii, Sov. Astron. Lett. **11** (1985), 271.
65) G. Efstathiou and J. R. Bond, Mod. Not R. Astron. Soc. **218** (1986), 103.
66) N. Vittorio, S. Matarrese and F. Lucchin, Astrophys. J. **328** (1988), 69.
67) K. M. Górski and J. Silk, Astrophys. J. Lett. **346** (1989), L1.
68) J. A. Holtzman, Astrophys. J. Suppl. **71** (1989), 1.
69) R. Scaramella and N. Vittorio, Astrophys. J. **353** (1990), 372.
70) L. F. Abbott and M. B. Wise, Astrophys. J. Lett. **282** (1984), L47.
71) E. L. Wright et al., Astrophys. J. Lett. **396** (1992), L13.
72) J. Yang, M. S. Turner, G. Steigman, D. N. Schramm and K. A. Olive, Astrophys. J. **281** (1984), 493.
73) J. R. GottIII et al., Astrophys. J. **352** (1990), 1.
74) A. Kashlinsky, Astrophys. J. **331** (1988), L1.
75) M. Sasaki, Mon. Not. R. Astron. Soc. **240** (1989), 415.
76) K. Tomita and K. Watanabe, Prog. Theor. Phys. **82** (1989), 563.
77) E. Kampen and E. Martínez-Gonzáles, 1991, preprint.
78) P. Annnios, R. A. Matzner, R. Tuluie and J. Centrella, Astrophys. J. **382** (1991), 71.
79) Ya. B. Zeldovich and R. A. Sunyaev, Astrophys. and Space Science **4** (1969), 301.
80) M. Birkinshaw, S. F. Gull and H. Hardebeck, Nature **309** (1984), 34.
81) S. T. Chase, R. D. Joseph, N. A. Robertson and P. A. R. Ade, Mon. Not. R. Astron. Soc. **225** (1987), 171.
82) U. Klein, Y. Raphneli, R. Schlickeiser and R. Wielebinski, Astron. and Astrophys. **244** (1991), 43.
83) M. Birkinshaw, in *Observational Cosmology*, IAU Symp. 124. (1987), p. 83.
84) N. Makino and Y. Suto, 1992, preprint.
85) T. Chiba et al., 1992, in preparation.
86) K. Sato, Mon. Not. R. Astron. Soc. **195** (1981), 467.
87) A. Gould, 1992, preprint.